iScience

CellPress
OPEN ACCESS

Article

A New Compound with Increased Antitumor Activity by Cotargeting MEK and Pim-1

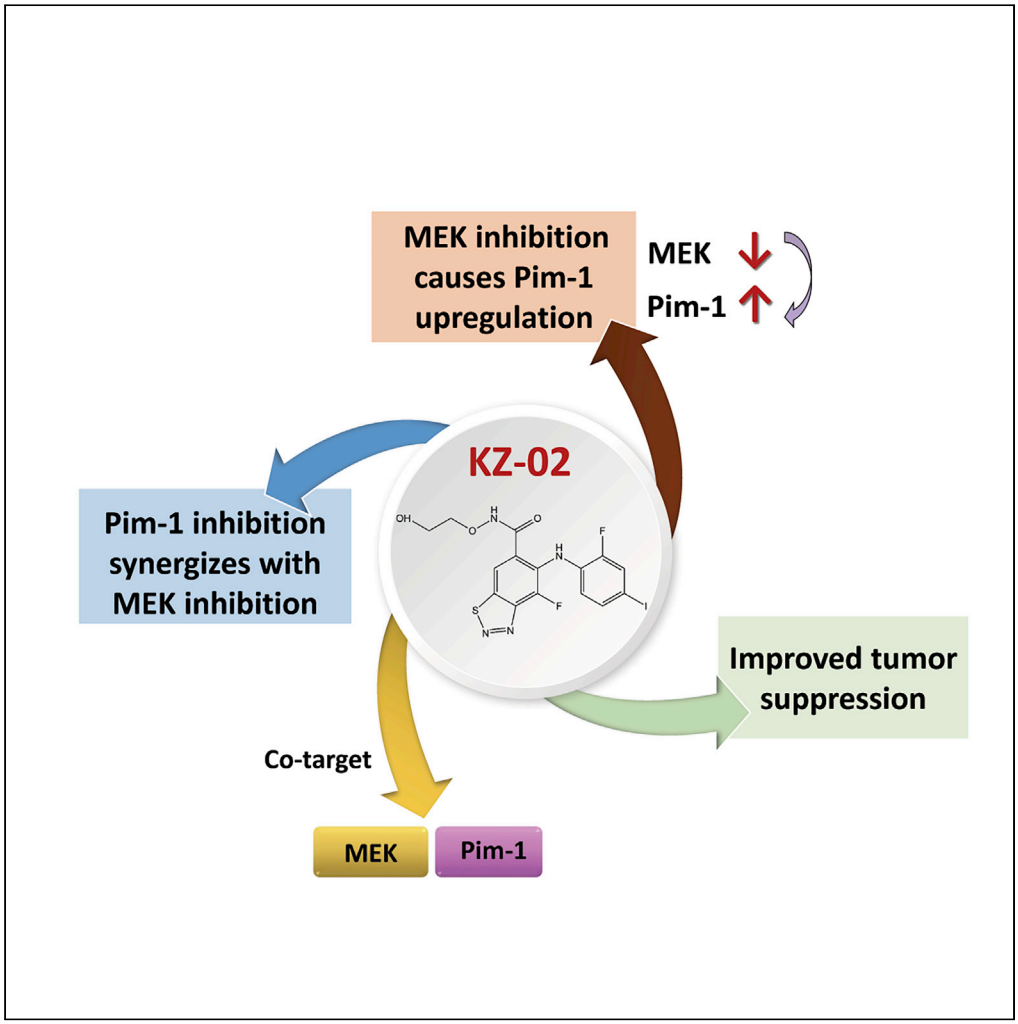

Yanan Li, Ying Cheng, Maoqi Zhang, ..., Hongqi Tian, Xiaomin Song, Yukun Cui

tianhongqi@irm-cams.ac.cn (H.T.)
xmsong01@sibcb.ac.cn (X.S.)
yukuncui@yahoo.com (Y.C.)

HIGHLIGHTS

Inhibition of MEK leads to Pim-1 upregulation

Pim-1 inhibition synergizes with MEK inhibition

A new compound is developed, which cotargets MEK and Pim-1

Li et al., iScience *23*, 101254
July 24, 2020 © 2020 The Authors.
https://doi.org/10.1016/j.isci.2020.101254

iScience

CellPress
OPEN ACCESS

Article

A New Compound with Increased Antitumor Activity by Cotargeting MEK and Pim-1

Yanan Li,[1,2,5] Ying Cheng,[3,5] Maoqi Zhang,[2,5] Xiaoli He,[4] Li Kong,[2] Kexiang Zhou,[2] Yunfu Zhou,[4] Lin Li,[4] Hongqi Tian,[3,*] Xiaomin Song,[4,*] and Yukun Cui[2,6,*]

SUMMARY

Feedback circuits are one of the major causes underlying tumor resistance. Thus, compounds that target one oncogenic pathway with simultaneously blocking its compensatory pathway will be of great value for cancer treatment. Here, we develop a new MEK inhibitor designated as KZ-02 that exhibits unexpectedly higher cytotoxicity than its starting compound AZD6244, a well-known MEK inhibitor, in colorectal cancer (CRC). Subsequent kinase selectivity study identified Pim-1 as an additional cellular target for KZ-02. Further studies showed that AZD6244 and Pim-1 1 (a Pim-1 inhibitor) have a synergistic effect on CRC suppression. Mechanistic study revealed that MEK inhibition by AZD6244 leads to increased Pim-1 expression, which could be a general mechanism behind the compromised cell-killing activity of MEK inhibitors. KZ-02, despite increasing Pim-1 mRNA expression, simultaneously promotes Pim-1 proteasomal degradation. Therefore, we uncover a new MEK inhibitor KZ-02 with significantly enhanced antitumor activity by co-targeting MEK and Pim-1.

INTRODUCTION

The RAS/ERK pathway involved in the control of cell proliferation and apoptosis regulation is deregulated in more than 30% of human cancers (Zhang et al., 2018; Zhao and Adjei, 2014). The narrow substrate specificity and distinctive structural characteristics render MEK1/2 ideal targets for therapeutic development (Duncan et al., 2015; Fischmann et al., 2009). Since 2000, when the first phase I study of a MEK inhibitor (CI-1040) was carried out by Lorusso and his colleagues (Lorusso et al., 2005), more than a dozen of highly specific and potent MEK1/2 inhibitors have been developed and evaluated in clinical studies (Decaudin et al., 2018; Finn et al., 2018). Despite the increasing number of MEK inhibitors identified, only trametinib (GSK212), cobimetinib (GDC-0973), and binimetinib (MEK162) have gained U S Food and Drug Administration (FDA) approval for clinical use (Signorelli and Shah Gandhi, 2017; Wright and McCormack, 2013). Other agents exhibit limited efficacy when used as a single agent and fail to demonstrate substantial clinical activity in treating tumors. One leading cause for this lack of efficacy is due to cross talks between ERK pathway and other pathways, such as PI3K-AKT pathway (Brighton et al., 2018). These have resulted in the clinical study of MEK inhibitors combined with inhibitors of PI3K, AKT, or mTOR (Fukumoto et al., 2018; Rosenberg et al., 2018; Wainberg et al., 2017). Despite the progress obtained, these agents are only efficacious in a limited range of cancers. Therefore, there is a great need to develop new MEK inhibitors and find mechanisms that confer tumor cell resistance to MEK inhibition.

The proviral integration site for moloney murine leukemia virus (Pim-1) is a serine/threonine (Ser/Thr) kinase. The activity of Pim-1 is exclusively dependent on its protein levels, which are controlled by gene transcription and proteasome-mediated degradation (Qian et al., 2005; Shay et al., 2005). Pim-1 displays oncogenic potential with upregulated expression in human malignancies of hematopoietic and epithelial origin (Brasó-Maristany et al., 2016). Pim-1 overexpression predicts worse outcome for several human malignancies, but it also correlates with better prognosis in human prostate and pancreatic cancers (Narlik-Grassow et al., 2013; Reiser-Erkan et al., 2008). Pim-1 is recognized as a therapeutic target, although serious side effects have stopped a clinical trial of one Pim-1 inhibitor (Cortes et al., 2018; Fan et al., 2017). Pim-1 is a critical effector mediating cross talks among different signaling pathways, especially those involving AKT and ERK (Le et al., 2016). It has been reported that Pim-1 plays an important role in the regulation of ERK pathway (Lin et al., 2010). Inhibition of Pim-1 is associated with increased ERK phosphorylation, suggesting

[1]College of Medical Imaging, Shanxi Medical University, Taiyuan, Shanxi 030001, China

[2]Guangdong Provincial Key Laboratory of Breast Cancer Diagnosis and Treatment, Shantou University Medical College Cancer Hospital, 7 Raoping Road, Shantou, Guangdong 515031, China

[3]Institute of Radiation Medicine, Chinese Academy of Medical Sciences and Peking Union Medical College, 238 Baidi Road, Tianjin 300192, China

[4]State Key Laboratory of Molecular Biology, CAS Center for Excellence in Molecular Cell Science, Shanghai Institute of Biochemistry and Cell Biology, Shanghai Institutes for Biological Sciences, Chinese Academy of Sciences, 320 Yueyang Road, Shanghai 200031, China

[5]These authors contributed equally

[6]Lead Contact

*Correspondence: tianhongqi@irm-cams.ac.cn (H.T.), xmsong01@sibcb.ac.cn (X.S.), yukuncui@yahoo.com (Y.C.)

https://doi.org/10.1016/j.isci.2020.101254

This is an open access article under the CC BY-NC-ND license (http://creativecommons.org/licenses/by-nc-nd/4.0/).

that activation of ERK-mediated survival pathways could result from Pim-1-targeted inhibition. However, whether the ERK/MAPK pathway may regulate Pim-1 activity remains unclear.

Herein, we developed a new MEK inhibitor designated as KZ-02 with AZD6244 as the starting point. KZ-02 showed ~5-fold greater kinase inhibitory activity than AZD6244. However, KZ-02 exhibited unexpectedly high cytotoxicity of three orders of magnitude more than AZD6244. This leads to identification of Pim-1 as an additional target for KZ-02. Further studies reveal that MEK inhibition leads to enhanced Pim-1 expression, which dampens the cell-killing ability of MEK inhibitors. However, KZ-02, despite increasing Pim-1 expression due to its inhibition of MEK activation, also promotes proteasome-dependent degradation of Pim-1, ultimately inhibiting Pim-1 activation.

RESULTS

Development of a New MEK Inhibitor KZ-02

The clinical importance of MEK signaling in human cancer and the limitations of existing MEK inhibitors promoted us to develop new MEK inhibitors. The starting point we used was the well-known MEK inhibitor AZD6244. AZD6244 has been reported to potently inhibit MEK1 with IC_{50} (50% inhibitory concentration) of 14 nmol/L (Yeh et al., 2007). It is currently under clinical evaluation as a single agent or in combination with other cytotoxic chemotherapy drugs or radiation therapy in various tumor types (Carvajal et al., 2018; Song et al., 2018; Tai et al., 2016). Based on the unsatisfactory potency of AZD6244, we proposed that a large substituent group on 3-nitrogen might result in a decreased antitumor activity. In addition, the de-methylation of 3-nitrogen methyl of AZD6244 could occur by *in vivo* enzyme metabolism (Dymond et al., 2016). Therefore, we replaced the 3-nitrogen methyl in the benzoheterocyclic ring of AZD6244 with S atom, generating a benzothiadiazole core. We also replaced the -Cl and -Br substituent on the aniline with -F and -I, respectively. The resulting new compound was designated as KZ-02 (Figure 1A). The step-by-step synthesis details for KZ-02 were described in Figure S1. The corresponding analysis spectra for key intermediates and target compound were presented in Data S1. A complex structure of MEK1/KZ-02 was built based on the MEK1/AZD6244 co-crystal structure (PDB code: 4U7Z) (Figure 1B). The replacement of the N-methyl by a smaller group of S atom may improve the affinity between KZ-02 and MEK1. Besides, compared with AZD6244 that has one H-bond accepting nitrogen for Ser212, KZ-02 has two on the thiadiazole ring (Figure 1B), which may facilitate the binding between KZ-02 and the Ser212 of MEK1. The iodine and fluorine atom on lipophilic ring of KZ-02 may also contribute to an improved affinity by modifying the interaction of KZ-02 with the Val127 and Lys97 of MEK1. As expected, KZ-02 indeed exhibited improved potency versus AZD6244 as reflected by *in vitro* kinase inhibition assay that was carried out as a commercial service by Cerep Drug Discovery Services Co. LTD (France). The IC_{50} for KZ-02 was 1.1 nmol/L, whereas the IC_{50} of AZD6244 was determined as 5.1 nmol/L (Figures 1C and 1D). Thus, we obtained a new compound, KZ-02, that is ~5-fold more potent than AZD6244 in MEK inhibition.

KZ-02 Exhibits Unexpectedly Higher Cytotoxicity over AZD6244

Next, we compared the inhibitory effect of KZ-02 and AZD6244 on colorectal cancer (CRC) cell growth. Two CRC cell lines, Colo205 and HT29, were used, and these two cell lines both harbor a constitutively activated RAS/ERK pathway (Janku, 2018). CRC cells were treated with increasing concentrations of compounds and cell proliferation was determined at 24, 48, and 72 h by using the MTT (methylthiazolyldiphenyl-tetrazolium bromide) method. KZ-02 significantly inhibited cell viability in a dose-dependent manner; moreover, KZ-02 exhibited higher activity than ADZ6244 in both CRC cell lines at nearly all time points (Figures 2A and 2B). The IC_{50} of KZ-02 against Colo205 and HT29 at 48 h were 0.015 and 4.1 nmol/L, respectively (Figure 2C). Compared with AZD6244, KZ-02 was three orders of magnitude more potent in inhibiting the growth of Colo205 cells (0.015 versus 15.5 nmol/L), whereas the IC_{50} of AZD6244 for inhibiting HT29 could not be determined at concentrations ranging from 0.01 to 1,000 nmol/L (Figure 2C). Considering the surprisingly increased superiority of KZ-02 to AZD6244 in MTT assay (~1,000-fold) compared with that in MEK inhibition assay (~5-fold), we suspected that KZ-02 might have cellular target(s) in addition to MEK.

To further evaluate the antitumor effect of KZ-02 *in vivo*, we generated Colo205 colon cancer xenograft to examine the antitumor effects of KZ-02. After 20 days of oral administration, KZ-02 inhibited Colo205 xenograft growth by 56.6% at a dosage of 1 mg/kg/day; by contrast, AZD6244 showed a similar inhibition when the dosage was used as high as 10 mg/kg/day (Figure 2D). Of note, even the highest dose of drugs tested in these experiments had no apparent effect on the body weight of tumor-bearing mice (Figure 2E). These results further confirmed the superior activity of KZ-02 over AZD6244.

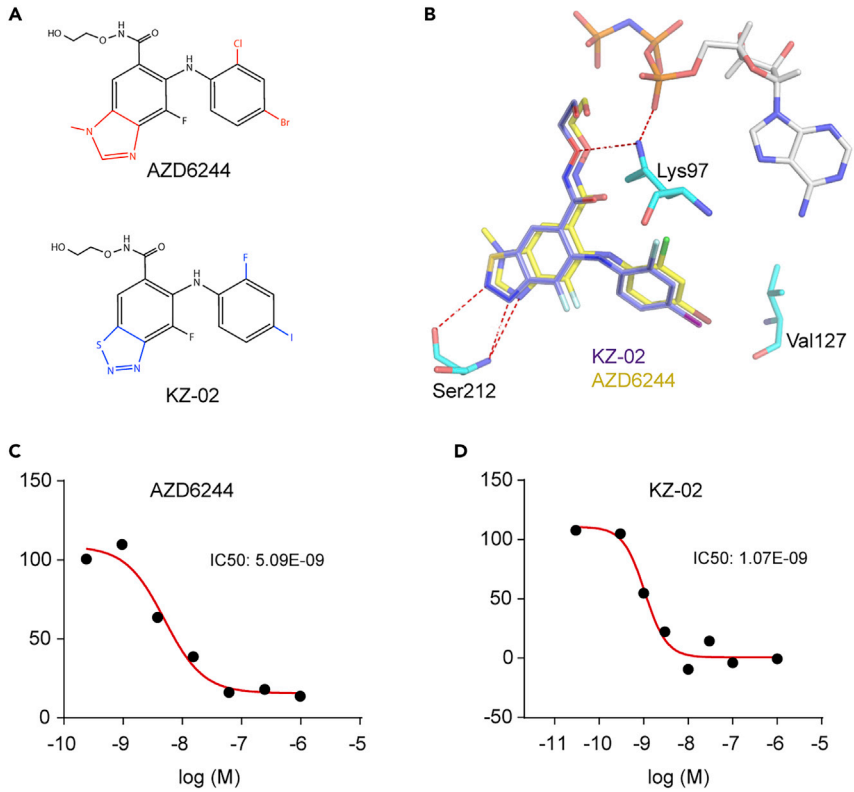

Figure 1. Development of a New MEK Inhibitor KZ-02

(A) Chemical structure of KZ-02 and AZD6244.

(B) KZ-02 structure (purple) overlapped with AZD6244 (yellow) with the co-crystal structure of MEK1/ATP/AZD6244 (PDB code: 4U7Z) as the model. KZ-02 shows similar binding with MEK1, and key residues of MEK1 that are important for interaction with KZ-02/AZD6244 are shown.

(C) In vitro kinase inhibition assay determines IC50 for AZD6244 to 5.09 nmol/L.

(D) In vitro kinase inhibition assay determines IC50 for KZ-02 to be 1.07 nmol/L. Data are represented as mean ± SD.

Pim-1 Is an Additional Target for KZ-02

To uncover possible additional targets of KZ-02, we used the commercial service provided by the Cerep Drug Discovery Services Co. LTD (France) to perform the kinase selectivity experiment for KZ-02. The inhibitory activity values were expressed as percent of inhibitory activity of 5 mmol/L stausporin, a pan kinase inhibitor. Among the selected 77 kinases, Pim-1 ranked the second only next to MEK1, exhibiting significantly higher sensitivity to KZ-02 than the rest of the kinases (Table S1). *In vitro* kinase inhibition assay determined the IC_{50} of KZ-02 against Pim-1 to be 1.34 μmol/L (Figure 3A). To further confirm the inhibition of KZ-02 toward Pim-1 kinase activity, we examined the effect of KZ-02 on the phosphorylation of Cdc25C, a known substrate of Pim-1 (Yuan et al., 2014). Treatment of KZ-02, in addition to blocking phosphorylation of ERK (the substrate for MEK), also led to inhibition of Cdc25C phosphorylation in both Colo205 and HT29 cells (Figure 3B). As expected, inhibition of Pim-1 activity by either Pim-1 1 (a Pim-1 inhibitor) or siRNA resulted in decreased phosphorylation of Cdc25C (Figure 3C). Together, these results demonstrate that KZ-02 is also an inhibitor for Pim-1.

Pim-1 Inhibition Has a Synergistic Effect with MEK Inhibition

If the additional Pim-1 inhibition accounts for the surprisingly high activity of KZ-02, it is reasonable to surmise that Pim-1 inhibition may increase the cell-killing efficiency of MEK inhibition. To test this possibility, we treated Colo205 and HT29 cells with AZD6244 and Pim-1 1, individually or in combination, for 24, 48, and 72 h. The inhibitory effects of these treatments on tumor cell growth were shown in Figures 4A and 4B. Of note, Pim-1 1 itself barely inhibited proliferation of both cell lines. We then calculated the coefficient of drug interaction (CDI), which is used to evaluate drug combination effect (Xu et al., 2007). We observed

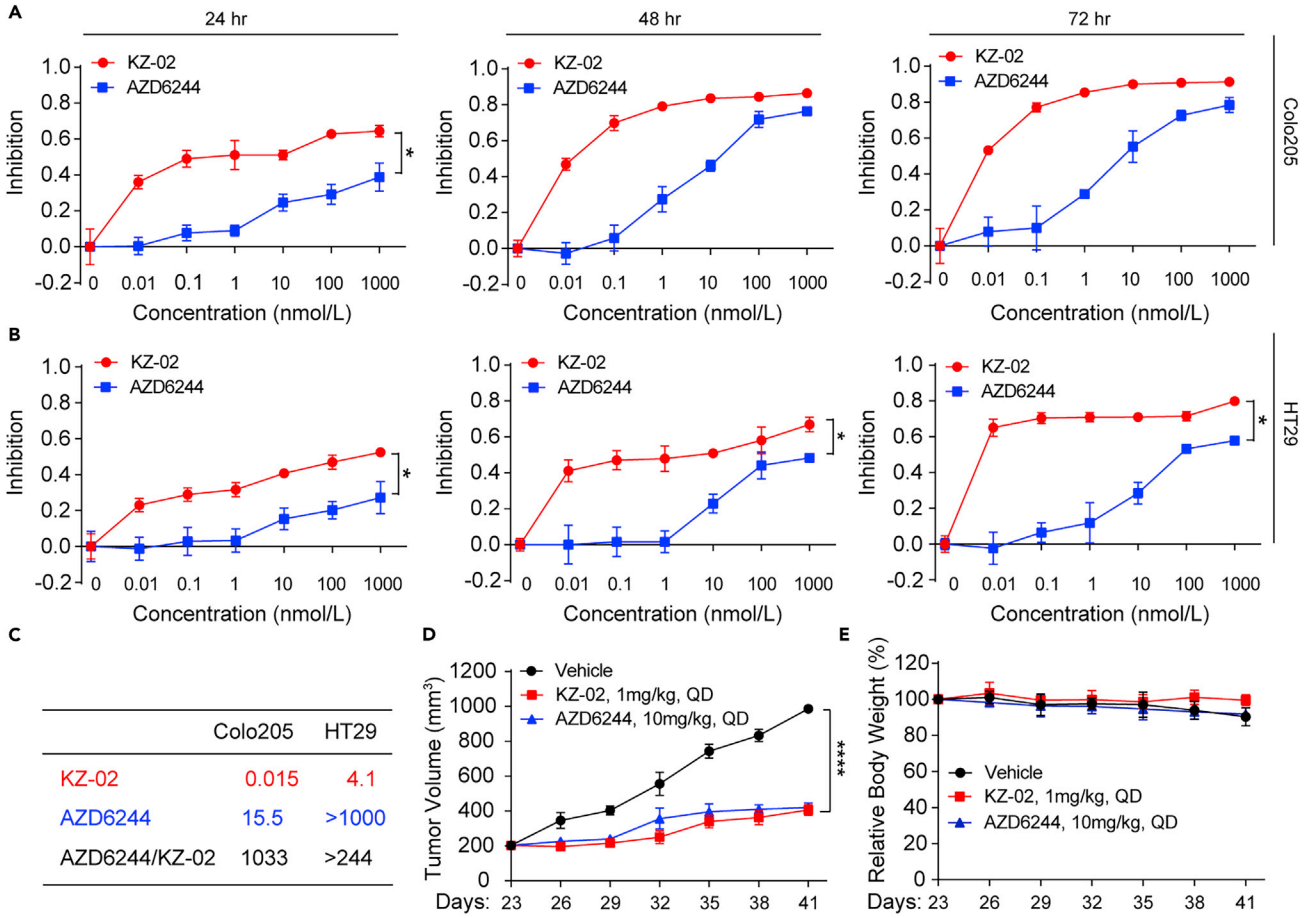

	Colo205	HT29
KZ-02	0.015	4.1
AZD6244	15.5	>1000
AZD6244/KZ-02	1033	>244

Figure 2. KZ-02 Exhibits Higher Activity Than AZD6244 in Inhibiting CRC Growth

(A and B) Examination of activity of KZ-02 versus AZD6244 in CRC cell growth inhibition. Colo205 (A) or HT29 (B) cells were treated with increasing concentrations of KZ-02 or AZD6244 and cell proliferation was determined at 24, 48, and 72 h by using the MTT method. Error bars are based on the standard deviations of triplicate samples.

(C) IC_{50} values for KZ-02 and AZD6244 calculated from data shown in (A) and (B), and the ratio of their IC_{50}s was also calculated.

(D) Examination of antitumor effects of KZ-02 versus AZD6244 in xenograft models. BALB/c mice were subcutaneously injected with 1×10^7 Colo205 cells. Mice were then randomly assigned to three groups (n = 8), vehicle, KZ-02, and AZD6244, which were orally administered once daily for 20 days. Tumor size and body weight were measured every 3 days from day 23 to day 41.

(E) Body weight variations of mice used in (D).

Data are represented as mean ± SD. Comparisons of two groups are performed with Student's t test. *$p < 0.05$, ****$p < 0.0001$.

a synergistic effect in both CRC cell lines (CDI<1), with significant synergy (CDI<0.7) occurring for most of Colo205 cell points and a portion of HT29 cell points (Figures 4C and 4D). This result suggested that Pim-1 1 has a synergistic action with AZD6244 in suppressing tumor cell growth.

To confirm the synergism between AZD6244 and Pim-1 1, we evaluated the *in vivo* antitumor efficacy of AZD6244 and Pim-1 1 in combination versus either agent alone by using the mouse xenograft model. AZD6244, Pim-1 1 or their combination was administered orally to HT29 cell-bearing mice. We found that the combination of AZD6244 and Pim-1 1 exhibited a significant improvement of tumor suppression compared with AZD6244 and Pim-1 1 used alone (Figure 4E). The minimum relative tumor volume (tumor volume on day 15/tumor volume on day 0) for AZD6244 plus Pim-1 1 was calculated to be 1.34 with CDI values all being less than one (Figure 4F). In comparison, the relative tumor volumes for AZD6244 and Pim-1 1 when used alone were 3.13 and 5.25, respectively, and the value for the vehicle control was 5.43. Negligible body weight fluctuations indicated few adverse effects of these therapeutic treatments on laboratory animals (Figure 4G). Taken together, these results showed that AZD6244 and Pim-1 1 have a synergistic effect on killing CRC tumor cells.

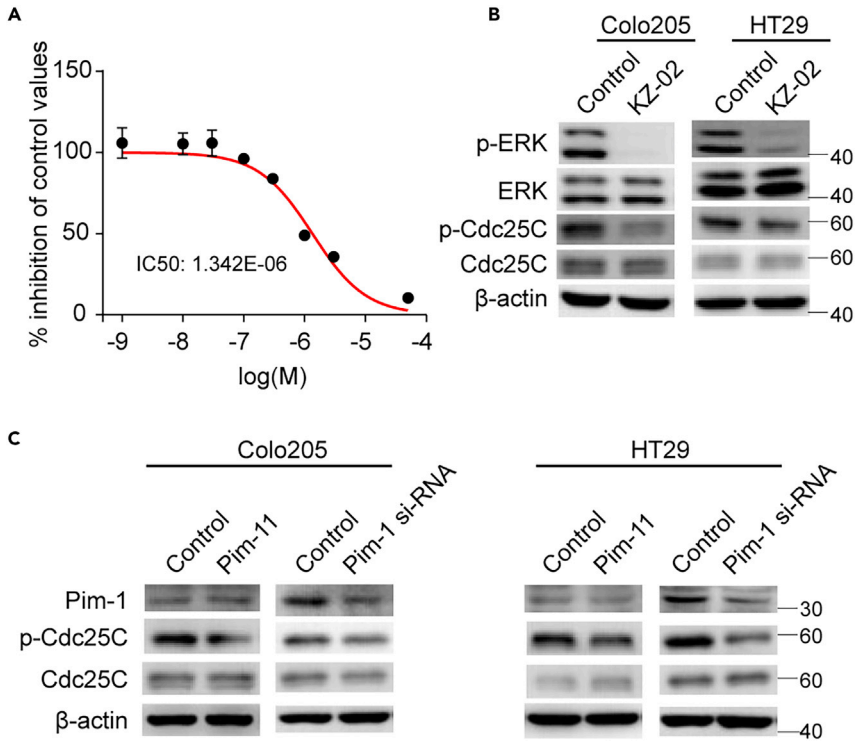

Figure 3. KZ-02 Additionally Targets Pim-1

(A) Kinase selectivity screening identified Pim-1 as an additional target for KZ-02 with IC_{50} being 1.34 μmol/L.

(B) Examination of KZ-02 inhibition on Pim-1 activity. Colo205 and HT29 cells were treated with KZ-02 (10 nmol/L) or DMSO (control) for 2 h, followed by western blot analysis. Cdc25C is a known substrate of Pim-1.

(C) Either Pim-1 1, a Pim-1 inhibitor, or Pim-1 siRNA treatment decreased Cdc25C phosphorylation. Cells were treated with 100 nmol/L Pim-1 1 for 2 h, or 40 nmol/L Pim-1 siRNA for 48 h, and then were lysed and subjected to western blot analysis. Data are represented as mean ± SD.

MEK Inhibition Resulted in Increased Pim-1 Expression

Next, we set out to investigate the mechanism behind such a synergistic action between MEK inhibition and Pim-1 inhibition. As mentioned before, inhibition of Pim-1 is previously reported to increase ERK phosphorylation (Lin et al., 2010). We asked whether ERK/MAPK pathway might affect Pim-1 activity in return. To test this possibility, we first examined the effect of AZD6244 treatment on Pim-1 expression in Colo205 and HT29 cells. As shown in Figure 5A, AZD6244 treatment (100 nmol/L) led to a decrease of ERK phosphorylation but an increase of Pim-1 protein expression and Cdc25C phosphorylation. Consistent with this, knockdown of ERK by siRNA produced similar results (Figure 5B). We then included two additional MEK inhibitors, trametinib and MEK162, which are both approved by FDA for cancer treatment, and tested their effects on Pim-1 expression in HT29 cells. Both MEK inhibitors inhibited ERK phosphorylation and meanwhile led to an increase of Pim-1 levels as did AZD6244 (Figure 5C). Together, these results suggest that MEK inhibition increases Pim-1 expression, which could be an inherent feature for MEK inhibitors.

To further confirm the effect of MEK inhibition on Pim-1 expression, we carried out *in vivo* analysis in HT29 cell-bearing mice. AZD6244 was administered orally at a dosage of 20 mg/kg/day for 15 days and then Pim-1 levels in control and AZD6244-treated tumor issues were analyzed by western blot analysis. As shown in Figure 5D, AZD6244 treatment led to a decrease of ERK phosphorylation, which was accompanied by an increase of Pim-1 protein levels. Finally, we examined the relationship of ERK phosphorylation levels and Pim-1 protein levels in serial slides of twenty clinical colon carcinoma specimens by immunohistochemistry (IHC). As shown in Figure 5E, ERK phosphorylation levels showed a negative correlation with Pim-1 protein levels in these clinical specimens with the negative correlation slope being −0.741. Consistently, quintessential ERK inhibition was associated with high Pim-1 positivity and vice versa as reflected by IHC assay (Figures 5F and 5G). Combined together, these results demonstrated that Pim-1 is subjected to negative regulation of ERK activation.

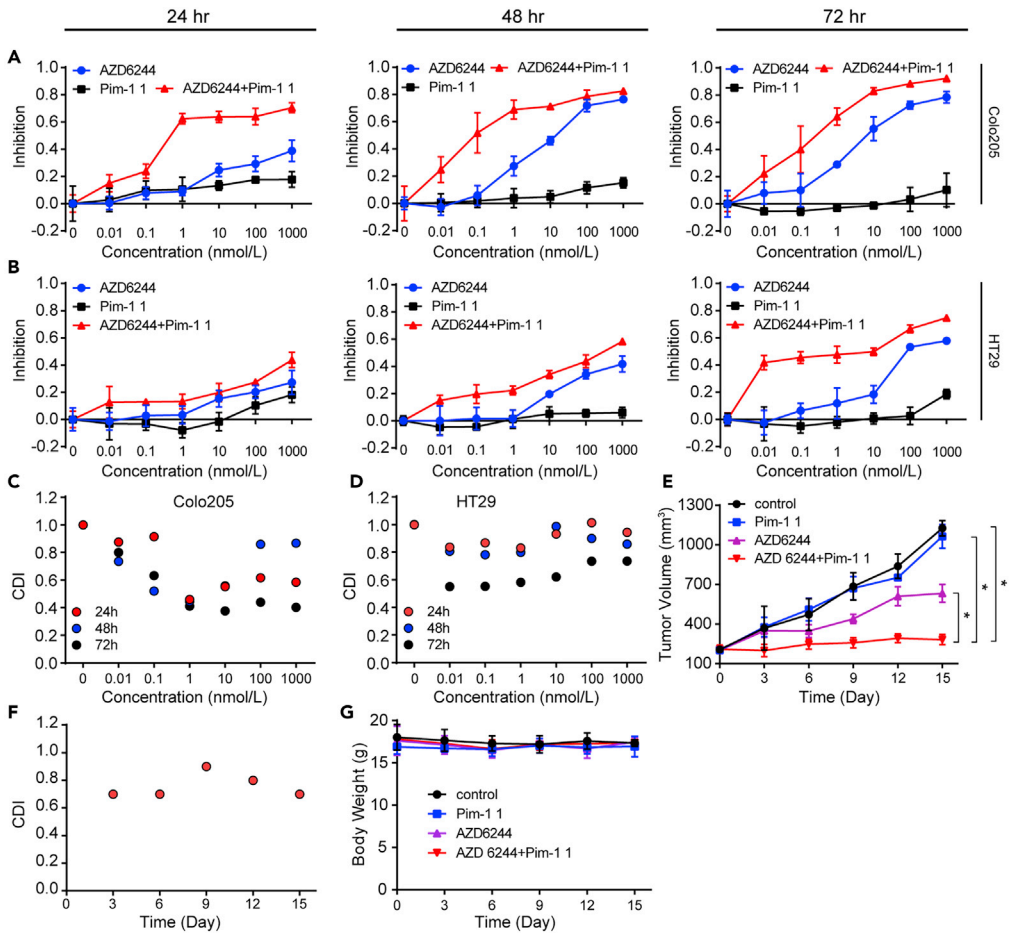

Figure 4. Pim-1 Inhibition Synergizes with MEK Inhibition in Inhibiting Tumor Growth

(A and B) AZD6244 and Pim-1 1 show synergism in inhibiting tumor cell growth. Colo205 (A) or HT29 (B) cells were treated with AZD6244 and Pim-1 1, individually or in combination (1:1, nmol/L), for 24, 48, and 72 h. The inhibitory effects of these treatments on tumor cell growth were then measured by the MTT assay.

(C) CDIs were calculated for data from (A).

(D) CDIs were calculated for data from (B).

(E) Evaluation of AZD6244 and Pim-1 1 combination in xenograft models. HT29 bearing xenograft mice were orally administrated with AZD6244 (20 mg/kg), Pim-1 1 (20 mg/kg), or their combination (both 20 mg/kg), and tumor volumes were examined every 3 days for 15 consecutive days.

(F) CDIs were calculated for data in (E).

(G) Body weights of experimental mice used in (E).

Error bars are based on the standard deviations of triplicate samples for *in vitro* cell viability test and eight duplicate results for *in vivo* tumor inhibition. Data are represented as mean ± SD. Comparisons of two groups are performed with Student's t test. *$p < 0.05$.

MEK Regulates Pim-1 via ERK/AMPK/IL-23/STAT3/Pim-1 Pathway

Next, we sought to explore the possible signal transduction cascade bridging ERK and Pim-1. Since interleukin-induced STAT3 activation is the major mechanism behind Pim-1 gene transactivation (Block et al., 2012), we first tested the effect of AZD6244 on the expression of interleukins. We treated HT29 cells with AZD6244 for 2 h (100 nmol/L) and examined by real-time PCR the expression of several interleukins (ILs), including IL-8, IL-10, IL-16, and IL-23, which have been reported to be expressed in CRC cells (Gao et al., 2009; Geng et al., 2017; Hu et al., 2017; Shi et al., 2016; Ting et al., 2013). We found that only IL-23 was significantly upregulated by AZD6244 (Figure 6A). IL-23 is a proinflammatory cytokine that is involved in many autoimmune diseases (Shi et al., 2016); moreover, IL-23 has been implicated in the progression of CRCs (Hu et al., 2017). Next, we investigated whether IL-23 may affect STAT3 phosphorylation and Pim-1 levels. We treated HT29 cells with recombinant IL-23 (10 ng/mL) for 2 h. As shown in Figure 6B, IL-23

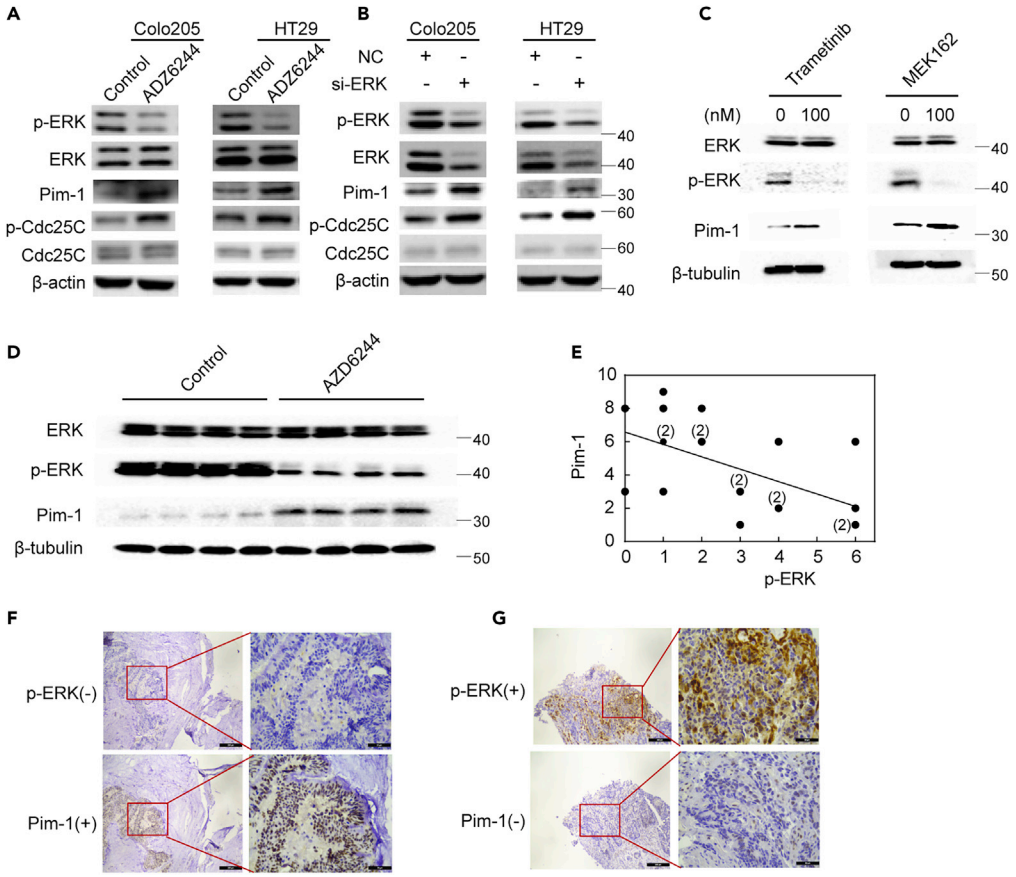

Figure 5. MEK Inhibition Increases Pim-1 Expression

(A) AZD6244 increases Pim-1 levels in CRC cells. Colo205 and HT29 cells were treated with AZD6244 (100 nmol/L) for 2 h, and expression of proteins was then detected by western blot analysis with indicated antibodies.

(B) Knockdown of ERK increases Pim-1 levels. CRC cells were incubated with 40 nmol/L of ERK1/2 siRNA or a scramble control siRNA for 48 h, and protein levels were detected by western blot analysis with indicated antibodies.

(C) Effects of two additional MEK inhibitors, trametinib and MEK162, on Pim-1 expression. HT29 cells were treated with trametinib (100 nmol/L) or MEK162 (100 nmol/L) for 2 h, and then cells were lysed and Pim-1 levels were detected by western blot analysis.

(D) The effect of MEK inhibition on Pim-1 expression in xenograft models. Four control or AZD6244-treated HT29 xenografted tumors were randomly selected to test the impact of AZD6244 on the expression of Pim-1 using western blot analysis.

(E) Correlation analysis of ERK phosphorylation levels and Pim-1 protein levels in 20 CRC patient tumor specimens. Clinical colon carcinoma specimens were analyzed by immunohistochemistry (IHC). The immunoreactive score (IRS) of Pim-1 versus p-ERK for each sample was calculated. Five IRSs that have overlapped ones were labeled.

(F) Representative image shows that reduced ERK phosphorylation corresponding to overexpression of Pim-1 in human colorectal tumors detected by IHC (solid red line indicated the enlarged view of the red box in each picture).

(G) Representative image shows that enhanced ERK phosphorylation corresponding to the reduction of Pim-1 expression in human colorectal tumors detected by IHC (solid red line indicated the enlarged view of the red box in each picture).

treatment increased STAT3 phosphorylation and Pim-1 expression, whereas knockdown of IL-23 by siRNA had a reverse effect. We then asked whether IL-23 is required for AZD6244-induced increase of Pim-1 expression. For this, we treated HT29 cells with AZD6244 combined with IL-23 siRNA. As shown in Figure 6C, AZD6244 treatment increased STAT3 phosphorylation and Pim-1 expression, whereas knockdown of IL-23 abrogated these effects of AZD6244 without affecting its inhibitory effect on ERK/AMPK pathway. Of note, AMPK activation lead to a decrease of IL-23 expression (Shi et al., 2016). Indeed, we observed that an AMPK-specific inhibitor (compound C) significantly increased the expression of IL-23, which is accompanied by an increase of STAT3 phosphorylation and Pim-1 levels; however, these effects could be reversed by knockdown of IL-23 (Figure 6D). Similarly, either MEK inhibition by AZD6244 or AMPK inhibition

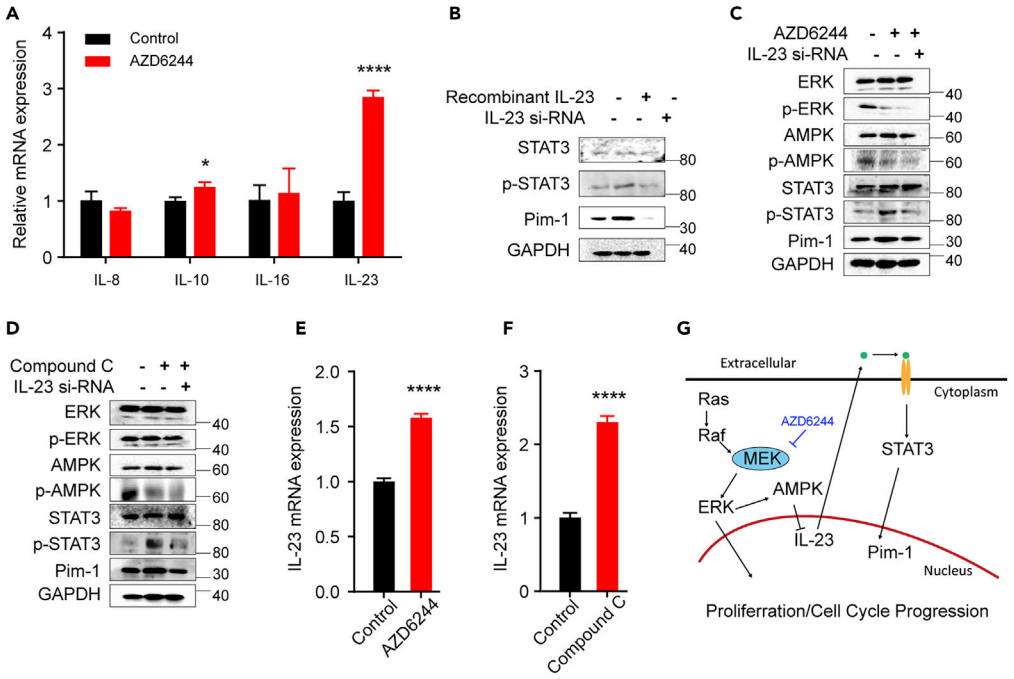

Figure 6. MEK Regulates Pim-1 via ERK/AMPK/IL-23/STAT3 Cascade

(A) IL-23 is specifically upregulated by AZD6244. HT29 cells were treated with AZD6244 (100 nmol/L) for 2 h, and mRNA levels of IL-8, IL-10, IL-16, and IL-23 were then detected by real-time PCR.

(B) HT29 cells were treated with recombinant IL-23 (10 ng/mL) for 2 h or IL-23 siRNA (50 nmol/L) for 48 h. STAT3 phosphorylation and Pim-1 expression were then detected by western blot analysis.

(C) HT29 cells were treated with AZD6244 (100 nmol/L) for 2 h with or without 48-h pretreatment with a scramble or IL-23 siRNA (50 nmol/L), and protein expression or phosphorylation levels were then detected by specific antibodies as indicated.

(D) Same experiment as (C) with AZD6244 replaced by an AMPK inhibitor, compound C.

(E) HT29 cells were treated either with AZD6244 (100 nmol/L) for 2 h, and then IL-23 expression was detected by real-time PCR.

(F) HT29 cells were treated either with compound C (40 μmol/L) for 2 h, and then IL-23 expression was detected by real-time PCR.

(G) Mechanistic model for MEK inhibition-induced Pim-1 upregulation. MEK inhibition increases IL-23 expression through ERK/AMPK signaling, which then activates STAT3, thereby promoting Pim-1 transactivation.

Data are represented as mean ± SD. Comparisons of two groups are performed with Student's t test. *$p < 0.05$, ****$p < 0.0001$.

by compound C led to an increase of IL-23 expression (Figures 6E and 6F). Taken together, these results reveal a feedback regulation of Pim-1 by MEK through ERK/AMPK/IL-23/STAT3/Pim-1 pathway, which accounts for MEK inhibitor-induced Pim-1 upregulation and thus confers tumor cell resistance to MEK inhibition (Figure 6G).

KZ-02 Inhibits Pim-1 Activation by Promoting Its Proteasomal Degradation

According to the findings above, as an MEK inhibitor, KZ-02 should increase Pim-1 expression. To verify this, we first assessed the effect of KZ-02 on Pim-1 protein levels in Colo205 and HT29 cells. However, unlike AZD6244, KZ-02 treatment decreased, rather than increased Pim-1 protein levels (Figure 7A). Intracellular Pim-1 protein levels were controlled by both transcriptional regulation and proteasome-mediated turn over. Considering the opposing effects of AZD6244 and KZ-02 on Pim-1 protein levels, we next compared them on their impact on Pim-1 transcriptional regulation and proteasome-mediated turn over. We first performed real-time PCR to examine possible effects of KZ-02 or AZD6244 on mRNA levels of Pim-1. MEK inhibition, either by KZ-02 or by AZD6244, is accompanied with an increase of Pim-1 mRNA levels in Colo205 cells and HT29 cells (Figures 7B and S2A). This result is consistent with our findings above that MEK inhibition leads to an increased Pim-1 expression.

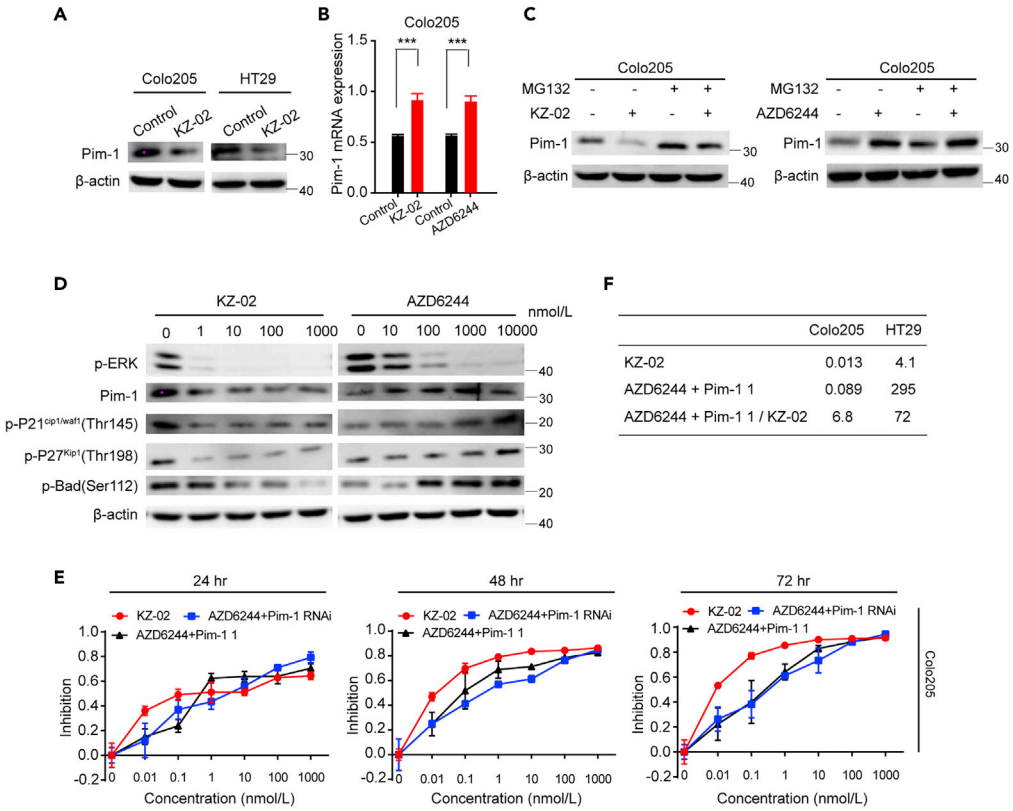

Figure 7. KZ-02 Inhibits Pim-1 Function by Promoting Its Proteasomal Degradation

(A) KZ-02 treatment decreases Pim-1 protein levels. Colo205 and HT29 cells were treated with KZ-02 (10 nmol/L) for 2 h, and Pim-1 protein levels were then detected by western blot analysis.

(B) Both KZ-02 and AZD6244 increase Pim-1 mRNA levels. Tumor cells were treated with KZ-02 (10 nmol/L) or AZD6244 (100 nmol/L) for 2 h, and Pim-1 mRNA levels were then analyzed by real-time PCR. Similar experiment in HT29 cells was shown in Figure S2A.

(C) Tumor cells were treated with either KZ-02 (10 nmol/L) or AZD6244 (100 nmol/L) for 2 h with or without addition of the proteasome inhibitor MG132 (10 μg/mL) for 30 min, and Pim-1 expression was then detected by western blot analysis. Similar experiment in HT29 cells was shown in Figure S2B.

(D) KZ-02 treatment inhibits Pim-1 and its downstream effectors, whereas AZD6244 increases their activation in Colo205 cells. Similar experiment in HT29 cells was shown in Figure S2D.

(E) Tumor cells were treated with various concentrations of KZ-02, AZD6244+Pim-1 1 (1:1), or AZD6244+Pim-1 siRNA (8 nmol/L) as indicated for 24, 48, and 72 h. MTT assay was then used to characterize the inhibition of tumor cell proliferation. Similar experiment in HT29 cells was shown in Figure S2E.

(F) IC_{50} values were calculated for data in (D) and the ratios of AZD6244+Pim-1 1 to KZ-02 IC_{50} were shown. Pim-1 knockdown efficiency was confirmed in Figure S2C. Error bars are based on the standard deviations of triplicate samples. Data are represented as mean ± SD. Comparisons of two groups are performed with Student's t test. ***$p < 0.001$.

Next, we examined whether these two compounds could affect the proteasomal degradation of Pim-1. We treated tumor cells with either KZ-02 (10 nmol/L) or AZD6244 (100 nmol/L) for 2 h with or without addition of the proteasome inhibitor MG132. Pre-incubation of cells with 10 μg/mL MG132 for 30 min did not affect the increase of Pim-1 protein expression induced by AZD6244; however, MG132 abrogated the KZ-02-mediated decrease of Pim-1 protein levels in both tumor cells (Figures 7C and S2B). These data suggested that, although both compounds upregulate Pim-1 mRNA levels, KZ-02 simultaneously promotes proteasome-dependent degradation of Pim-1.

It has been reported that Pim-1 is involved in cell-cycle regulation through phosphorylating $P21^{Cip1/Waf1}$/$P27^{Kip1}$ (Morishita et al., 2008; Zhang et al., 2007). Moreover, Pim-1 could phosphorylate Bad to affect cell apoptosis (Aho et al., 2004). To further confirm different effects on Pim-1 activation by KZ-02 and AZD6244, we examined their effects on activation of $P21^{Cip1/Waf1}$/$P27^{Kip1}$ as well as Bad in

Colo205 cells or HT29 cells. As shown in Figures 7D and S2D, although both compounds inhibited ERK phosphorylation, they exhibited opposite effects on activation of $P21^{Cip1/Waf1}$/$P27^{Kip1}$ and Bad. KZ-02 lead to decreased Pim-1 levels, accompanied by decreased phosphorylation of $P21^{Cip1/Waf1}$/$P27^{Kip1}$ and Bad; instead, AZD6244 increased phosphorylation of $P21^{Cip1/Waf1}$/$P27^{Kip1}$ and Bad. These results further confirmed our conclusion that KZ-02 inhibits Pim-1 activation, whereas AZD6244 increases it.

We then compared the antitumor activity of KZ-02 with that of AZD6244 and Pim-1 1 in combination via the MTT assay. The combination of AZD6244 and Pim-1 siRNA was also included for comparison. The effective Pim-1 knockdown by siRNA was confirmed (Figure S2C). KZ-02 exhibited higher cell-killing ability than either the combination of AZD6244 plus Pim-1 1 (red versus black lines) or the combination of AZD6244 and Pim-1 siRNA (red versus blue lines) in both CRC cell lines (Figures 7E and S2E). We then calculated IC_{50} values for KZ-02 and AZD6244 plus Pim-1 1 at 48 h of treatment, respectively. The ratio of IC_{50} value of AZD6244+Pim-1 1 versus KZ-02 was 6.8 and 72 for Colo205 and HT29 cells, respectively (Figure 7F). These results showed that KZ-02, as a dual-target inhibitor, is more effective than the combination of AZD6244 and Pim-1 1 in inhibiting CRC tumor cell growth.

Finally, we examined whether KZ-02 exclusively targets tumor cells. A potential drug candidate for cancer therapy should specifically target tumor cells with normal and benign cells spared. As shown above, KZ-02 exerted a minimal or tolerable effect on the body weight of the experimental animals (Figure 2E). To further confirm that KZ-02 specifically targets tumor cells while sparing normal or benign cells, we evaluated the potential toxicity of KZ-02, AZD6244, Pim-1 1, or AZD6244+Pim-1 1 on the immortalized normal colon cell line (CCD841CoN) over a range of dosages (0.0–10,000 nmol/L) by using the MTT assay. The corresponding tumor cell line Colo205 was used as a control (0.0–1,000 nmol/L). As shown in Figure S2F, more than 95% of cells in the benign cells remained viable after 48 h of treatment with any of the above compounds, or their combination, even at a concentration as high as 10,000 nmol/L. By contrast, in tumor cells, a combination of AZD6244 and Pim-1 1 exhibited a concentration-dependent cell-killing activity beginning at concentration as low as 0.01 nmol/L, which was more potent compared with AZD6244 alone, but weaker than KZ-02; Pim-1 1, consistent with our results above, and had no apparent cell-killing activity when used alone (Figure S2G). Combined together, these results showed that KZ-02 specifically inhibits tumor cell growth with better performance than the combination of AZD6244 and Pim-1 1.

DISCUSSION

A recent large retrospective study detected mutations in the RAS/ERK pathway for nearly half of the patients with CRC (Lee et al., 2018), suggesting that MEK-targeted therapy could benefit a great number of patients with CRC. However, the development of acquired resistance, predominantly caused by reciprocal feedback of signal transduction pathways, will inevitably result in tumor recurrence in many cases. Understanding the feedback mechanisms underlying acquired resistance would thus facilitate the development of more effective drugs, as well as clinically relevant neoadjuvant regimens to improve the efficacy of anticancer treatment.

In this study, we initially aimed at developing a new MEK inhibitor based on the structure of the well-known MEK inhibitor AZD6244. However, the observation that KZ-02 shows remarkably more superiority to AZD6244 in the MTT assay than in the kinase assay urged us to explore the potential mechanism underlying the surprisingly high inhibitory activity of KZ-02. By using an *in vitro* kinase screening, we identified Pim-1 as an additional target for KZ-02. To our knowledge, this is the first MEK/Pim-1 dual-target inhibitor reported. Of note, KZ-02 shows less superiority over AZD6244 in xenograft mice model (~10-fold) than in the MTT assay (~1,000-fold). This is likely due to the inferior oral bioavailability of KZ-02 in mouse models. Further studies of pharmacokinetics and pharmacodynamics for KZ-02 would be required for evaluating and improving "drug-like" properties of KZ-02.

Pim-1 activity is dependent on its protein levels, which are controlled by transcription as well as by proteasomal degradation. Our data showed that both AZD6244 and KZ-02 increased Pim-1 mRNA levels, which could be a general mechanism underlying a compromised cell-killing ability of MEK inhibitors. Consistent with an elevation of Pim-1 activity following MEK inhibition, we find that AZD6244 induces cellular phosphorylation of Cdc25C, a substrate of Pim-1. This provides evidence that MEK pathway plays an important role in the feedback regulation of Pim-1. Further mechanistic studies revealed that inhibition of MEK could impede AMPK-mediated repression of IL-23 expression through decreasing phosphorylation of AMPK, which

subsequently upregulates the transcription of Pim-1 by activating STAT3. It has been reported that Pim-1 inhibition could activate ERK (Lin et al., 2010). Thus, our study herein reveals a reciprocal feedback loop between ERK and Pim-1. In the current study, the Pim-1 inhibitor Pim-1 1 alone exhibits no apparent inhibition against CRC tumor cells. However, when combined with AZD6244, Pim-1 1 displays a synergistic effect with AZD6244 on killing tumor cells both *in vitro* and *in vivo*. Although further clinical studies are required to address the effectiveness of this combination in treating patients with CRC, our data here clearly demonstrated that Pim-1 is an important survival factor that affects MEK-targeted treatment of CRCs, thereby identifying Pim-1 as a druggable target for enhancing the sensitivity of CRCs to MEK inhibitors. Moreover, our findings that MEK inhibition leads to AMPK suppression and STAT3 activation also suggest a possible synergistic effect between MEK inhibitors and AMPK activators or STAT3 inhibitors in CRC treatment.

KZ-02, despite increasing Pim-1 mRNA levels owing to its inhibition of MEK, causes a decrease of Pim-1 protein levels. Further studies revealed that KZ-02 could promote proteasome-dependent Pim-1 degradation. This unique activity of KZ-02 as a dual-target inhibitor endows it with superior performance to AZD6244, and even to a combination of AZD6244 and Pim-1 1. Thus far, the mechanism by which KZ-02 mediates proteasomal degradation of Pim-1 remains unknown. Pim-1 protein stability is largely dependent on its associated molecular chaperones, Hsp90 or Hsp70. Hsp90-bound Pim-1 is more stable, whereas an association with Hsp70 will lead to ubiquitination and degradation of Pim-1 (Shay et al., 2005). Thus, one possibility is that KZ-02 may switch Pim-1 to a conformation that prefers an interaction with Hsp70. The mechanism behind how KZ-02 mediates Pim-1 degradation warrants further studies.

In conclusion, this study shows that Pim-1 activation is an important factor contributing to tumor cell desensitization to MEK inhibitors, rendering Pim-1 as a druggable target in MEK-targeted cancer therapy. Combination of Pim-1 and MEK inhibitors may serve as an effective anticancer strategy to improve CRC treatment. Moreover, a new MEK/Pim-1 dual-target inhibitor KZ-02 is developed, which exhibits a high tumor cell-killing activity by simultaneously inhibiting ERK phosphorylation and promoting proteasome-dependent Pim-1 degradation.

Limitations of the Study

In this study, we developed a new MEK inhibitor that exhibits significantly improved antitumor activity by simultaneously targeting Pim-1. The new MEK inhibitor, designated as KZ-02, inhibits Pim-1 kinase activity as reflected by the kinase selectivity assay and the *in vitro* kinase inhibition assay. Notably, in addition to inhibiting Pim-1 kinase activity, we found that KZ-02 also decreases Pim-1 protein levels by promoting proteasomal degradation of Pim-1. Considering a mild inhibitory activity of KZ-02 against Pim-1 in the *in vitro* kinase inhibition assay but a significantly improved tumor cell-killing activity compared with AZD6244 as reflected by the MTT assay and the mouse tumor growth assay, we tend to believe that KZ-02 inhibits Pim-1 activity mainly through decreasing Pim-1 protein levels rather than inhibiting its kinase activity directly. However, so far, the cellular target and molecular mechanism behind the KZ-02-mediated Pim-1 degradation remain unclear, which absolutely warrant further investigations.

Resource Availability

Lead Contact

Dr. Yukun Cui (yukuncui@yahoo.com).

Materials Availability

Materials are available from the corresponding author on request.

Data and Code Availability

All data are available in the main text or in Supplemental Information.

METHODS

All methods can be found in the accompanying Transparent Methods supplemental file.

SUPPLEMENTAL INFORMATION

Supplemental Information can be found online at https://doi.org/10.1016/j.isci.2020.101254.

ACKNOWLEDGMENTS

We thank Dr. Stanley Lin for his critical editing. This work was supported by Strategic priority research program of CAS (XDB19000000) to L.L., National Natural Science Foundation of China (81903662) to Y.L., National Natural Science Foundation of China (31571456) to X.S., National Natural Science Foundation of China (81272931, 81572588) the running open grant of Guangdong Provincial Key Laboratory for Breast Cancer Diagnosis & Treatment (2017B030314116), Guangdong Provincial Special Fund of Sci-tech Innovation Strategy, Key Disciplinary Project of Clinical Medicine under the Guangdong High-level University Development Program, and an open grant from the State Key Laboratory of Molecular Biology to Yukun Cui.

AUTHOR CONTRIBUTIONS

Y.L. performed most of the *in vitro* experiments and participated in manuscript preparation. Ying Cheng synthesized KZ-02 and contributed to manuscript preparation. M.Z. conducted part of mechanistic studies, assisted with clinical sample collection, and participated in xenograft model-related experiments. X.H. assisted with experimental design. L.K. and K.Z. contributed to validation of the selectivity of KZ-02. Y.Z. contributed to data interpretation. L.L. contributed to the design of the study. H.T. designed KZ-02 and assisted with project supervision. X.S. participated in project supervision and manuscript preparation. Yukun Cui conceived this study, organized the collaboration, obtained financial support, and participated in manuscript preparation.

DECLARATION OF INTERESTS

H.T. has filed patents regarding KZ-02. No potential conflicts of interest were disclosed by the other authors.

Received: March 19, 2020
Revised: May 26, 2020
Accepted: June 5, 2020
Published: July 24, 2020

REFERENCES

Aho, T.L., Sandholm, J., Peltola, K.J., Mankonen, H.P., Lilly, M., and Koskinen, P.J. (2004). Pim-1 kinase promotes inactivation of the pro-apoptotic Bad protein by phosphorylating it on the Ser112 gatekeeper site. FEBS Lett. *571*, 43–49.

Block, K.M., Hanke, N.T., Maine, E.A., and Baker, A.F. (2012). IL-6 stimulates STAT3 and Pim-1 kinase in pancreatic cancer cell lines. Pancreas *41*, 773–781.

Brasó-Maristany, F., Filosto, S., Catchpole, S., Marlow, R., Quist, J., Francesch-Domenech, E., Plumb, D.A., Zakka, L., Gazinska, P., Liccardi, G., et al. (2016). PIM1 kinase regulates cell death, tumor growth and chemotherapy response in triple-negative breast cancer. Nat. Med. *22*, 1303–1313.

Brighton, H.E., Angus, S.P., Bo, T., Roques, J., Tagliatela, A.C., Darr, D.B., Karagoz, K., Sciaky, N., Gatza, M.L., Sharpless, N.E., et al. (2018). New mechanisms of resistance to MEK inhibitors in melanoma revealed by intravital imaging. Cancer Res. *78*, 542–557.

Carvajal, R.D., Piperno-Neumann, S., Kapiteijn, E., Chapman, P.B., Frank, S., Joshua, A.M., Piulats, J.M., Wolter, P., Cocquyt, V., Chmielowski, B., et al. (2018). Selumetinib in combination with dacarbazine in patients with metastatic uveal melanoma: a phase III, multicenter, randomized trial (SUMIT). J. Clin. Oncol. *36*, 1232–1239.

Cortes, J., Tamura, K., DeAngelo, D.J., de Bono, J., Lorente, D., Minden, M., Uy, G.L., Kantarjian, H., Chen, L.S., Gandhi, V., et al. (2018). Phase I studies of AZD1208, a proviral integration Moloney virus kinase inhibitor in solid and haematological cancers. Br. J. Cancer *118*, 1425–1433.

Decaudin, D., El Botty, R., Diallo, B., Massonnet, G., Fleury, J., Naguez, A., Raymondie, C., Davies, E., Smith, A., Wilson, J., et al. (2018). Selumetinib-based therapy in uveal melanoma patient-derived xenografts. Oncotarget *9*, 21674–21686.

Duncan, K.E., Chang, L.Y., and Patronas, M. (2015). MEK inhibitors: a new class of chemotherapeutic agents with ocular toxicity. Eye (Lond) *29*, 1003–1012.

Dymond, A.W., Howes, C., Pattison, C., So, K., Mariani, G., Savage, M., Mair, S., Ford, G., and Martin, P. (2016). Metabolism, excretion, and pharmacokinetics of selumetinib, an MEK1/2 inhibitor, in healthy adult male subjects. Clin. Ther. *38*, 2447–2458.

Fan, R.F., Lu, Y., Fang, Z.G., Guo, X.Y., Chen, Y.X., Xu, Y.C., Lei, Y.M., Liu, K.F., Lin, D.J., Liu, L.L., et al. (2017). PIM-1 kinase inhibitor SMI-4a exerts antitumor effects in chronic myeloid leukemia cells by enhancing the activity of glycogen synthase kinase 3beta. Mol. Med. Rep. *16*, 4603–4612.

Finn, R.S., Ahn, D.H., Javle, M.M., Tan, B.R., Jr., Weekes, C.D., Bendell, J.C., Patnaik, A., Khan, G.N., Laheru, D., Chavira, R., et al. (2018). Phase 1b investigation of the MEK inhibitor binimetinib in patients with advanced or metastatic biliary tract cancer. Invest. New Drugs *36*, 1037–1043.

Fischmann, T.O., Smith, C.K., Mayhood, T.W., Myers, J.E., Reichert, P., Mannarino, A., Carr, D., Zhu, H., Wong, J., Yang, R.S., et al. (2009). Crystal structures of MEK1 binary and ternary complexes with nucleotides and inhibitors. Biochemistry *48*, 2661–2674.

Fukumoto, S., Kanbara, K., and Neo, M. (2018). Synergistic anti-proliferative effects of mTOR and MEK inhibitors in high-grade chondrosarcoma cell line OUMS-27. Acta Histochem. *120*, 142–150.

Gao, L.B., Rao, L., Wang, Y.Y., Liang, W.B., Li, C., Xue, H., Zhou, B., Sun, H., Li, Y., Lv, M.L., et al. (2009). The association of interleukin-16 polymorphisms with IL-16 serum levels and risk of colorectal and gastric cancer. Carcinogenesis *30*, 295–299.

Geng, R., Tan, X., Wu, J., Pan, Z., Yi, M., Shi, W., Liu, R., Yao, C., Wang, G., Lin, J., et al. (2017). RNF183 promotes proliferation and metastasis of colorectal cancer cells via activation of NF-κB-IL-8 axis. Cell Death Dis. *8*, 2994–3004.

Hu, W.H., Chen, H.H., Yen, S.L., Huang, H.Y., Hsiao, C.C., and Chuang, J.H. (2017). Increased expression of interleukin-23 associated with

progression of colorectal cancer. J. Surg. Oncol. *115*, 208–212.

Janku, F. (2018). Advances on the BRAF front in colorectal cancer. Cancer Discov. *8*, 389–391.

Le, X., Antony, R., Razavi, P., Treacy, D.J., Luo, F., Ghandi, M., Castel, P., Scaltriti, M., Baselga, J., and Garraway, L.A. (2016). Systematic functional characterization of resistance to PI3K inhibition in breast cancer. Cancer Discov. *6*, 1134–1147.

Lee, S.K., Hwang, J.H., and Choi, K.Y. (2018). Interaction of the Wnt/β-catenin and RAS-ERK pathways involving co-stabilization of both β-catenin and RAS plays important roles in the colorectal tumorigenesis. Adv. Biol. Regul. *68*, 46–54.

Lin, Y.W., Beharry, Z.M., Hill, E.G., Song, J.H., Wang, W., Xia, Z., Zhang, Z., Aplan, P.D., Aster, J.C., Smith, C.D., et al. (2010). A small molecule inhibitor of Pim protein kinases blocks the growth of precursor T-cell lymphoblastic leukemia/lymphoma. Blood *115*, 824–833.

Lorusso, P.M., Adjei, A.A., Varterasian, M., Gadgeel, S., Reid, J., Mitchell, D.Y., Hanson, L., DeLuca, P., Bruzek, L., Piens, J., et al. (2005). Phase I and pharmacodynamic study of the oral MEK inhibitor CI-1040 in patients with advanced malignancies. J. Clin. Oncol. *23*, 5281–5293.

Morishita, D., Katayama, R., Sekimizu, K., Tsuruo, T., and Fujita, N. (2008). Pim kinases promote cell cycle progression by phosphorylating and down-regulating $p27^{Kip1}$ at the transcriptional and posttranscriptional levels. Cancer Res. *68*, 5076–5085.

Narlik-Grassow, M., Blanco-Aparicio, C., Cecilia, Y., Perez, M., Munoz-Galvan, S., Canamero, M., Renner, O., and Carnero, A. (2013). Conditional transgenic expression of PIM1 kinase in prostate induces inflammation-dependent neoplasia. PLoS One *8*, 60277–60289.

Qian, K.C., Wang, L., Hickey, E.R., Studts, J., Barringer, K., Peng, C., Kronkaitis, A., Li, J., White, A., Mische, S., et al. (2005). Structural basis of constitutive activity and a unique nucleotide binding mode of human Pim-1 kinase. J. Biol. Chem. *280*, 6130–6137.

Reiser-Erkan, C., Erkan, M., Pan, Z., Bekasi, S., Giese, N.A., Streit, S., Michalski, C.W., Friess, H., and Kleeff, J. (2008). Hypoxia-inducible proto-oncogene Pim-1 is a prognostic marker in pancreatic ductal adenocarcinoma. Cancer Biol. Ther. *7*, 1352–1359.

Rosenberg, L., Yoon, C.H., Sharma, G., Bertagnolli, M.M., and Cho, N.L. (2018). Sorafenib inhibits proliferation and invasion in desmoid-derived cells by targeting Ras/MEK/ERK and PI3K/Akt/mTOR pathways. Carcinogenesis *39*, 681–688.

Shay, K.P., Wang, Z., Xing, P.X., McKenzie, I.F., and Magnuson, N.S. (2005). Pim-1 kinase stability is regulated by heat shock proteins and the ubiquitin-proteasome pathway. Mol. Cancer Res. *3*, 170–181.

Shi, Q., Yin, Z., Liu, P., Zhao, B., Zhang, Z., Mao, S., Wei, T., Rao, M., Zhang, L., and Wang, S. (2016). Cilostazol suppresses IL-23 production in human dendritic cells via an AMPK-dependent pathway. Cell Physiol. Biochem. *40*, 499–508.

Signorelli, J., and Shah Gandhi, A. (2017). Cobimetinib. Ann. Pharmacother. *51*, 146–153.

Song, H., Zhang, J., Ning, L., Zhang, H., Chen, D., Jiao, X., and Zhang, K. (2018). The MEK1/2 inhibitor AZD6244 sensitizes BRAF-mutant thyroid cancer to vemurafenib. Med. Sci. Monit. *24*, 3002–3010.

Tai, W.M., Yong, W.P., Lim, C., Low, L.S., Tham, C.K., Koh, T.S., Ng, Q.S., Wang, W.W., Wang, L.Z., Hartono, S., et al. (2016). A phase Ib study of selumetinib (AZD6244, ARRY-142886) in combination with sorafenib in advanced hepatocellular carcinoma (HCC). Ann. Oncol. *27*, 2210–2215.

Ting, W.C., Chen, L.M., Huang, L.C., Hour, M.J., Lan, Y.H., Lee, H.Z., You, B.J., Chang, T.Y., and Bao, B.Y. (2013). Impact of interleukin-10 gene polymorphisms on survival in patients with colorectal cancer. J. Korean Med. Sci. *28*, 1302–1306.

Wainberg, Z.A., Alsina, M., Soares, H.P., Brana, I., Britten, C.D., Del Conte, G., Ezeh, P., Houk, B., Kern, K.A., Leong, S., et al. (2017). A multi-arm phase I study of the PI3K/mTOR inhibitors PF-04691502 and gedatolisib (PF-05212384) plus irinotecan or the MEK inhibitor PD-0325901 in advanced cancer. Target Oncol. *12*, 775–785.

Wright, C.J., and McCormack, P.L. (2013). Trametinib: first global approval. Drugs *73*, 1245–1254.

Xu, S.P., Sun, G.P., Shen, Y.X., Peng, W.R., Wang, H., and Wei, W. (2007). Synergistic effect of combining paeonol and cisplatin on apoptotic induction of human hepatoma cell lines. Acta Pharmacol. Sin. *28*, 869–878.

Yeh, T.C., Marsh, V., Bernat, B.A., Ballard, J., Colwell, H., Evans, R.J., Parry, J., Smith, D., Brandhuber, B.J., Gross, S., et al. (2007). Biological characterization of ARRY-142886 (AZD6244), a potent, highly selective mitogen-activated protein kinase kinase 1/2 inhibitor. Clin. Cancer Res. *13*, 1576–1583.

Yuan, L.L., Green, A.S., Bertoli, S., Grimal, F., Mansat-De Mas, V., Dozier, C., Tamburini, J., Recher, C., Didier, C., and Manenti, S. (2014). Pim kinases phosphorylate Chk1 and regulate its functions in acute myeloid leukemia. Leukemia *28*, 293–301.

Zhang, X., Liu, G., Ding, L., Jiang, T., Shao, S., Gao, Y., and Lu, Y. (2018). HOXA3 promotes tumor growth of human colon cancer through activating EGFR/Ras/Raf/MEK/ERK signaling pathway. J. Cell. Biochem. *119*, 2864–2874.

Zhang, Y., Wang, Z., and Magnuson, N.S. (2007). Pim-1 kinase-dependent phosphorylation of $p21^{Cip1/WAF1}$ regulates its stability and cellular localization in H1299 cells. Mol. Cancer Res. *5*, 909–922.

Zhao, Y., and Adjei, A.A. (2014). The clinical development of MEK inhibitors. Nat. Rev. Clin. Oncol. *11*, 385–400.

iScience, Volume *23*

Supplemental Information

A New Compound with Increased Antitumor Activity by Cotargeting MEK and Pim-1

Yanan Li, Ying Cheng, Maoqi Zhang, Xiaoli He, Li Kong, Kexiang Zhou, Yunfu Zhou, Lin Li, Hongqi Tian, Xiaomin Song, and Yukun Cui

SUPPLEMENTAL FIGURES

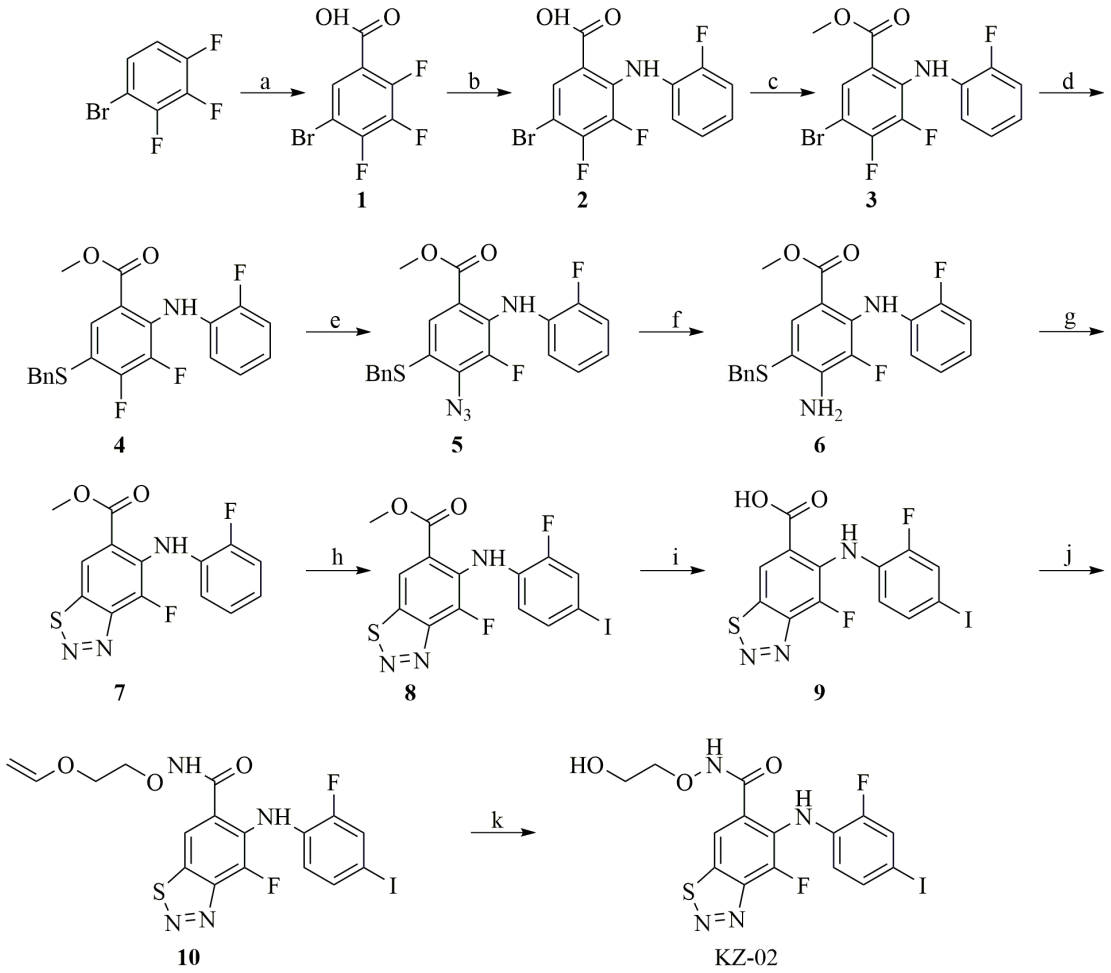

Figure S1. The Synthesis Route of KZ-02. The Analysis Spectra for Key Intermediates and Target Compound are Shown Below. Related to Figure 1.

(a) N_2, LDA, dry ice, dry THF, –78ºC to r.t. (b) N_2, 2-fluoroaniline, LiHMDS, –78ºC to r.t. (c) Thionyl chloride, 85ºC; DCM, Methanol, 0ºC. (d) N_2, phenylmethanethiol, DIPEA, Xantphos, Tris (dibenzylideneacetone) dipalladium, 1,4-dioxane, 90ºC. (e) NaN_3, DMA, 90ºC. (f) H_2, 10% Pd/C, Methanol, r.t. (g) con. HCl, H_2O, r.t; $NaNO_2/H_2O$, 10 ºC. (h) NIS, TFA, DMF, r.t. (i) 1M LiOH, THF/MeOH=4/1(v/v), r.t. (j) O-(2-(vinyloxy) ethyl) hydroxylamine, EDCI, HOBT, DCM, r.t. (k) 1M HCl, DCM, r.t. Abbreviations: LDA, Lithium diisopropylamide; THF, Tetrahydrofuran; LiHMDS, lithium hexamethyldisilamide; DCM, dichloromethane; DIPEA, N, N-Diisopropylethylamine; DMA, Dimethylacetamide; TFA, Trifluoroacetic acid; DMF, N, N-dimethyllformamide; EDCI, 1-Ethyl-3-(3-dimethylaminopropyl) carbetamide; NIS, N-Iodosuccinimide; HOBt, Hydroxybenzotriazole; r.t., room temperature. Analysis spectra for key intermediates and target compound are shown in

Data S1.

Data S1. Analysis Spectra for Key Intermediates and Target Compound. Related to Figure S1.

^{1}H NMR spectra of compound **1**

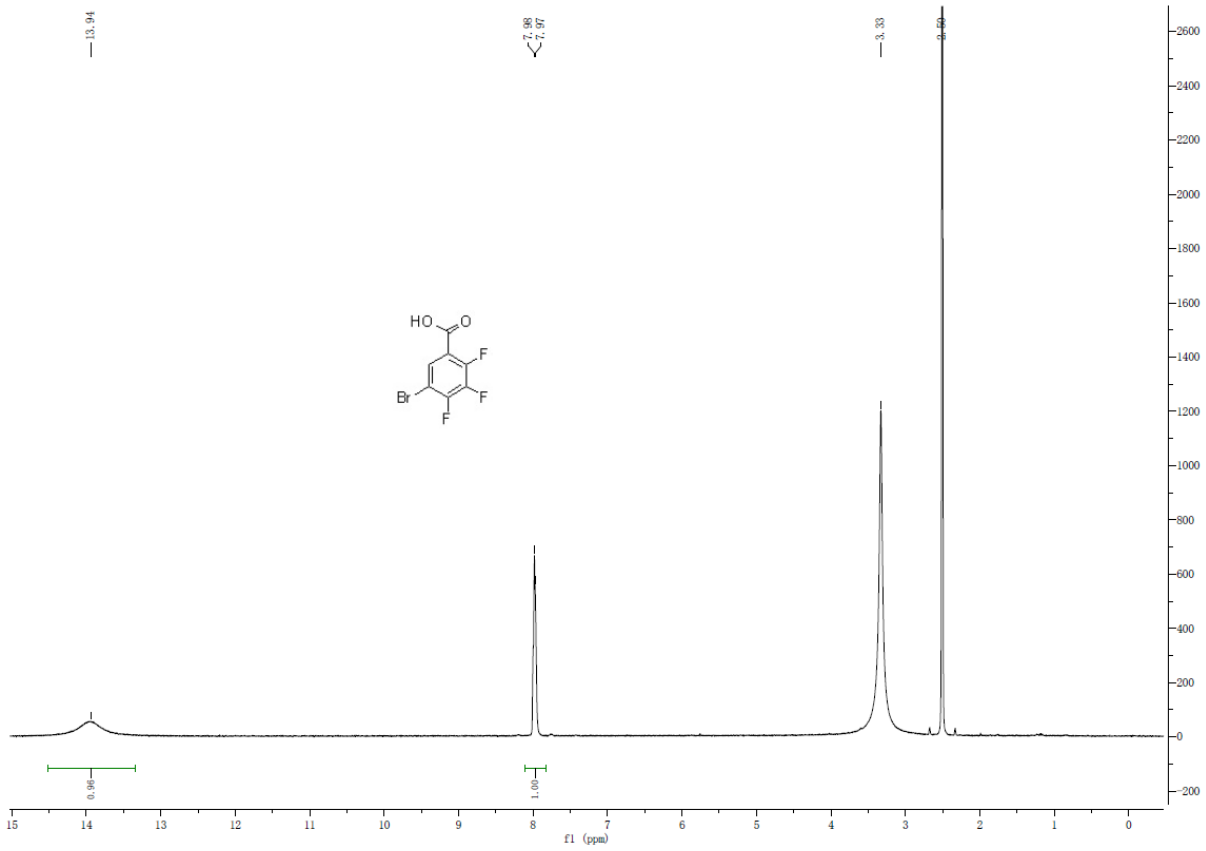

^{1}H NMR spectra of compound **2**

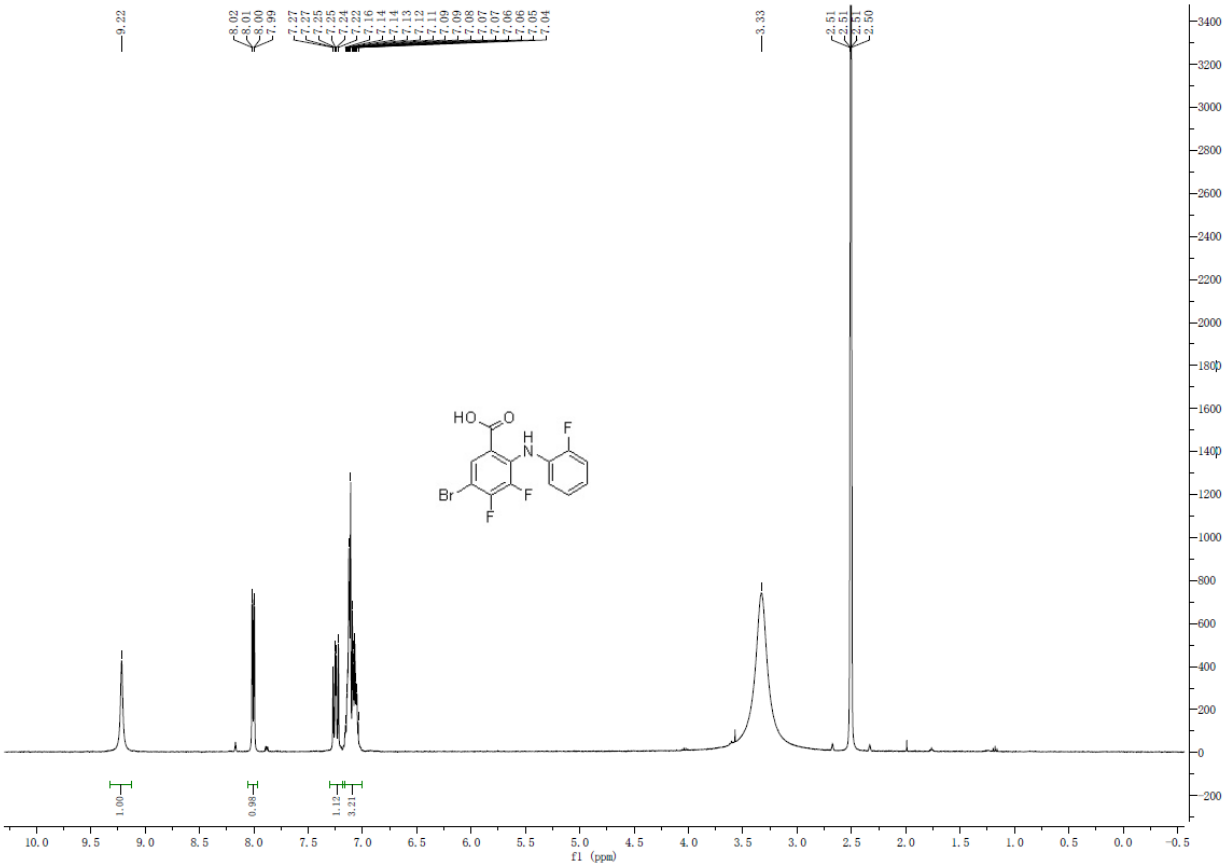

^{1}H NMR spectra of compound **3**

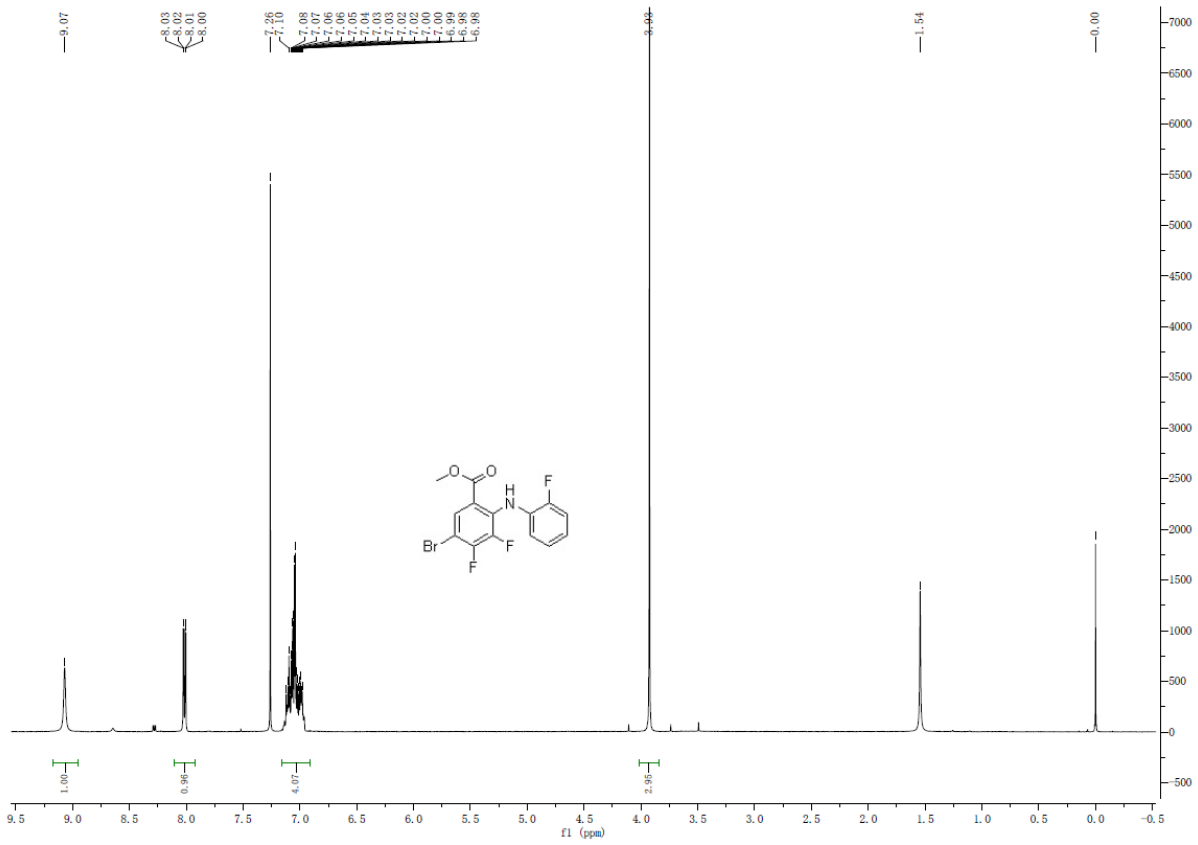

^{1}H NMR spectra of compound **4**

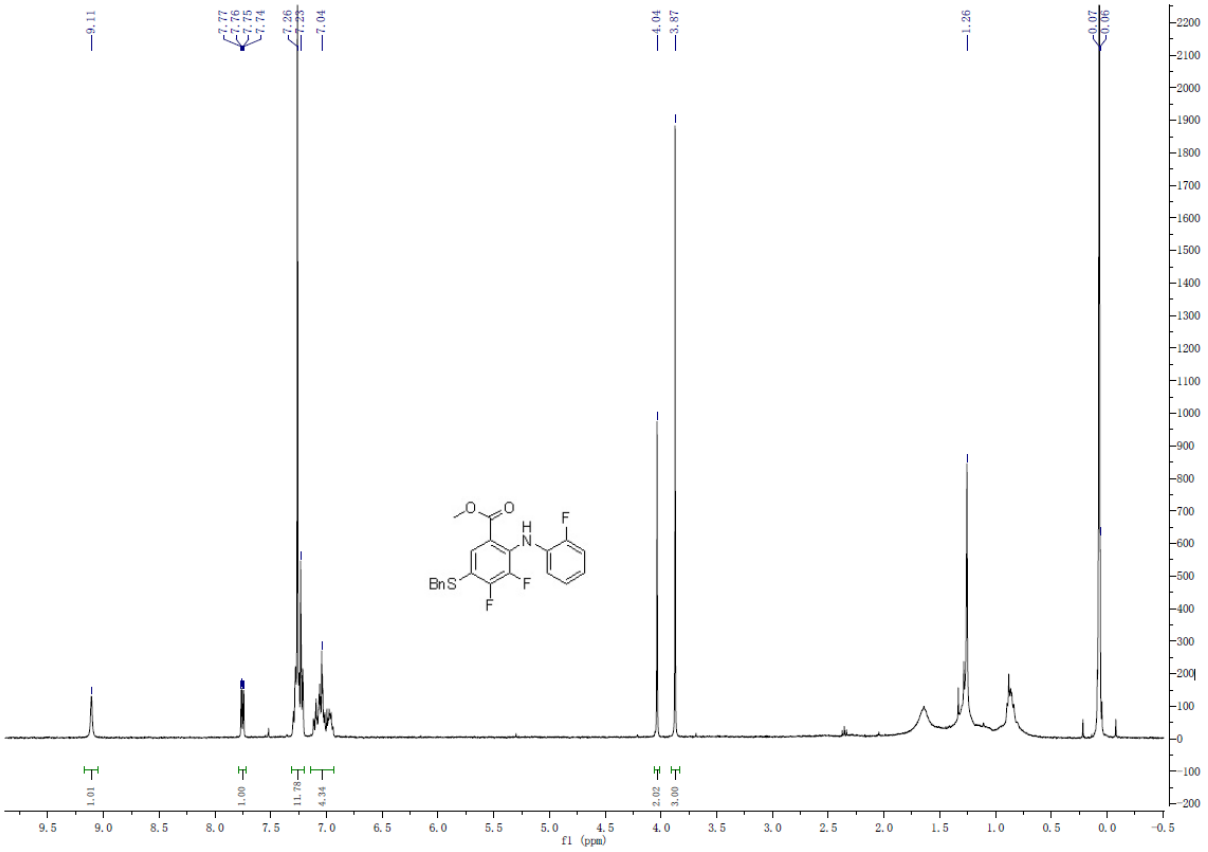

^{1}H NMR spectra of compound **5**

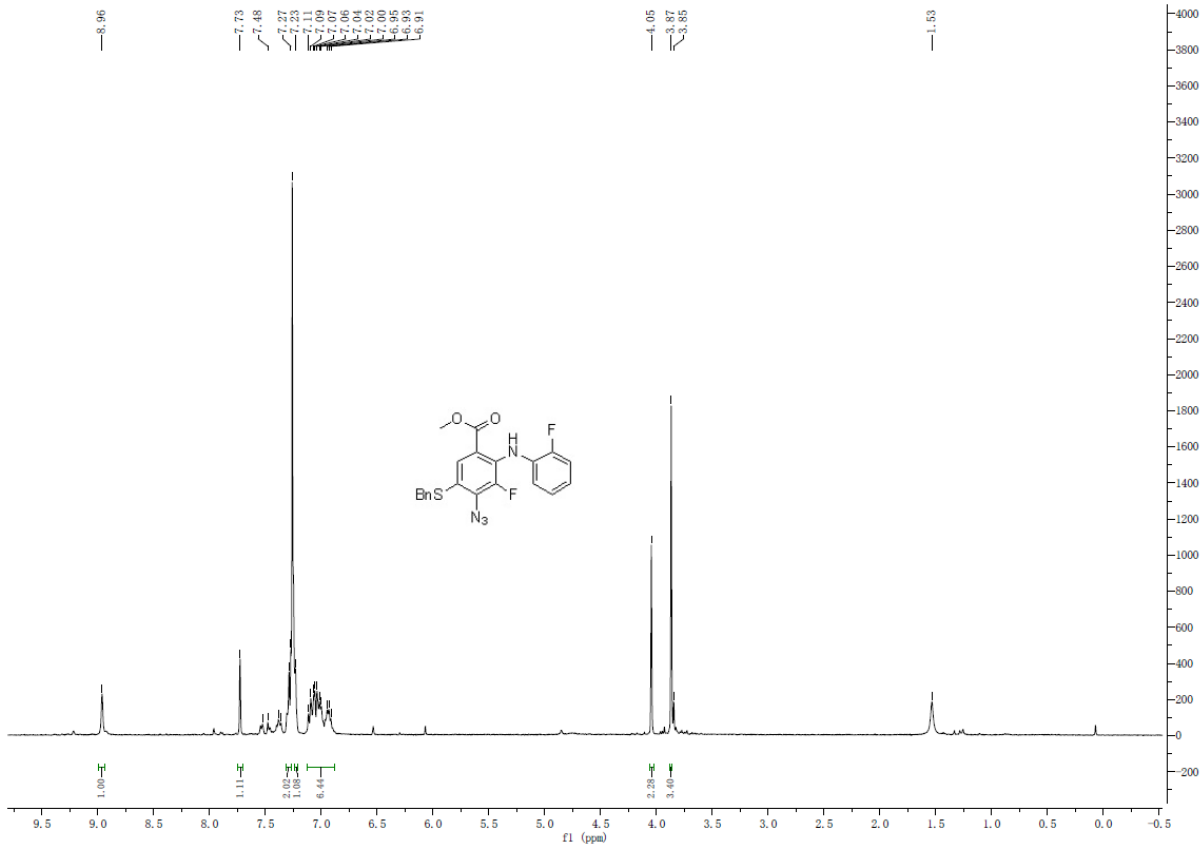

^{1}H NMR spectra of compound **7**

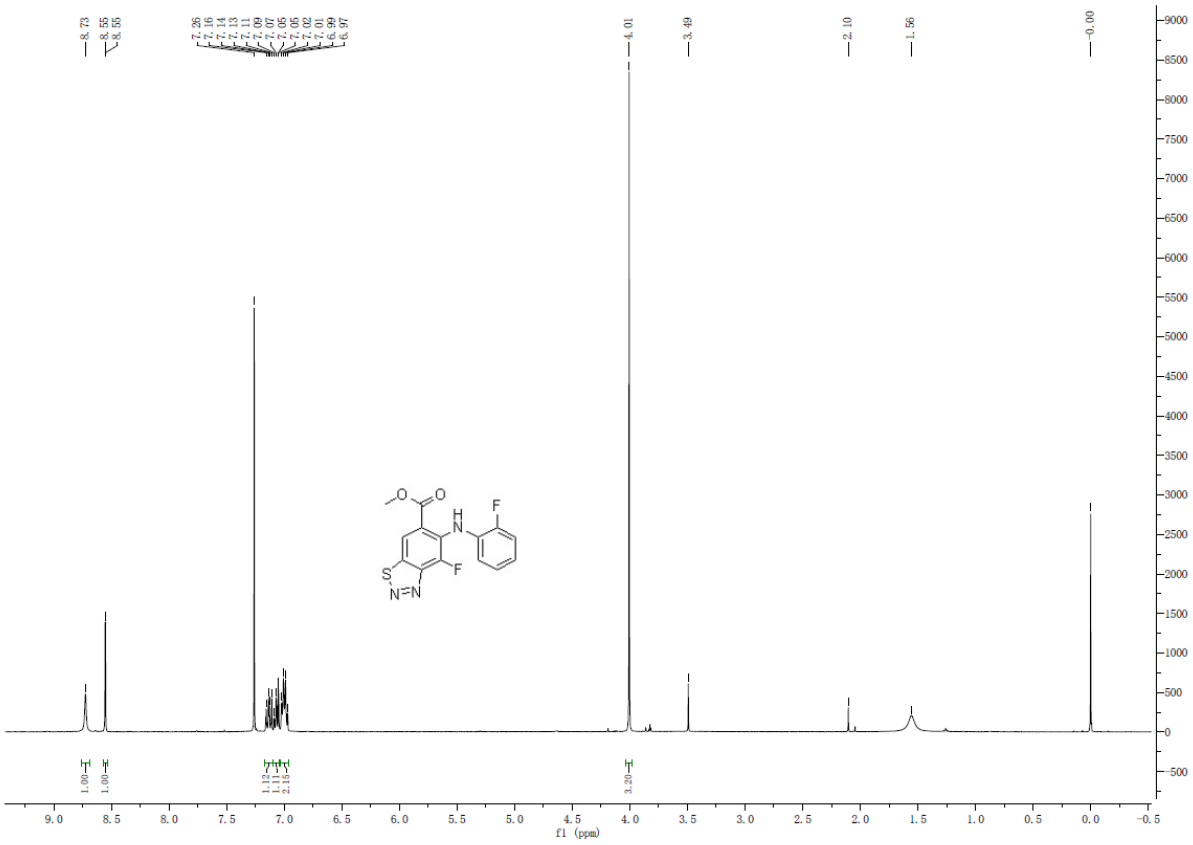

MS spectra of compound **7**

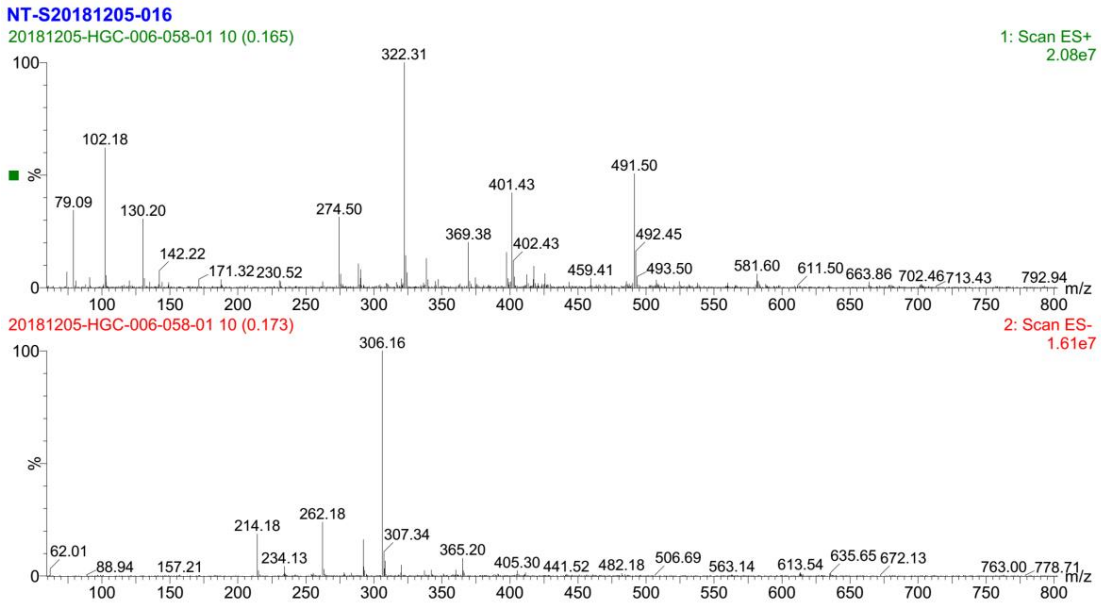

^{1}H NMR spectra of compound **8**

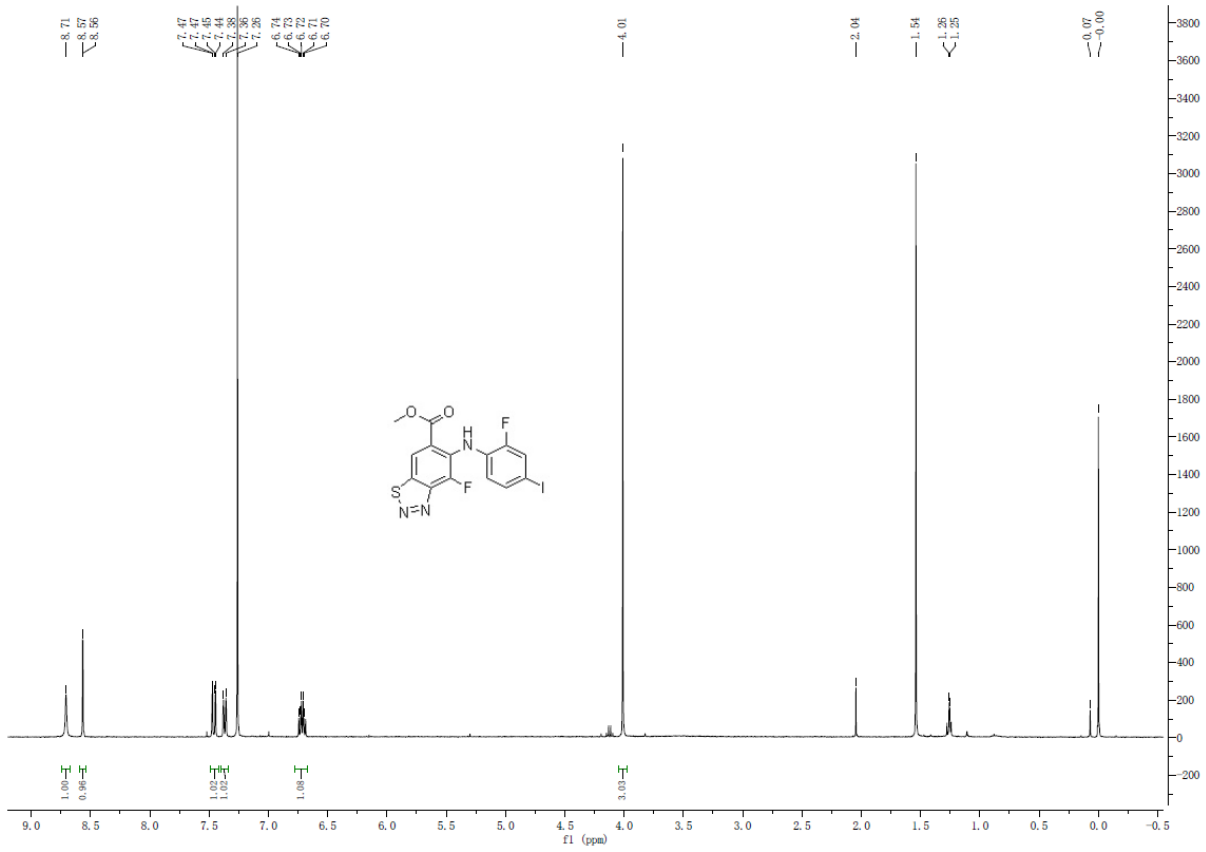

^{1}H NMR spectra of compound **9**

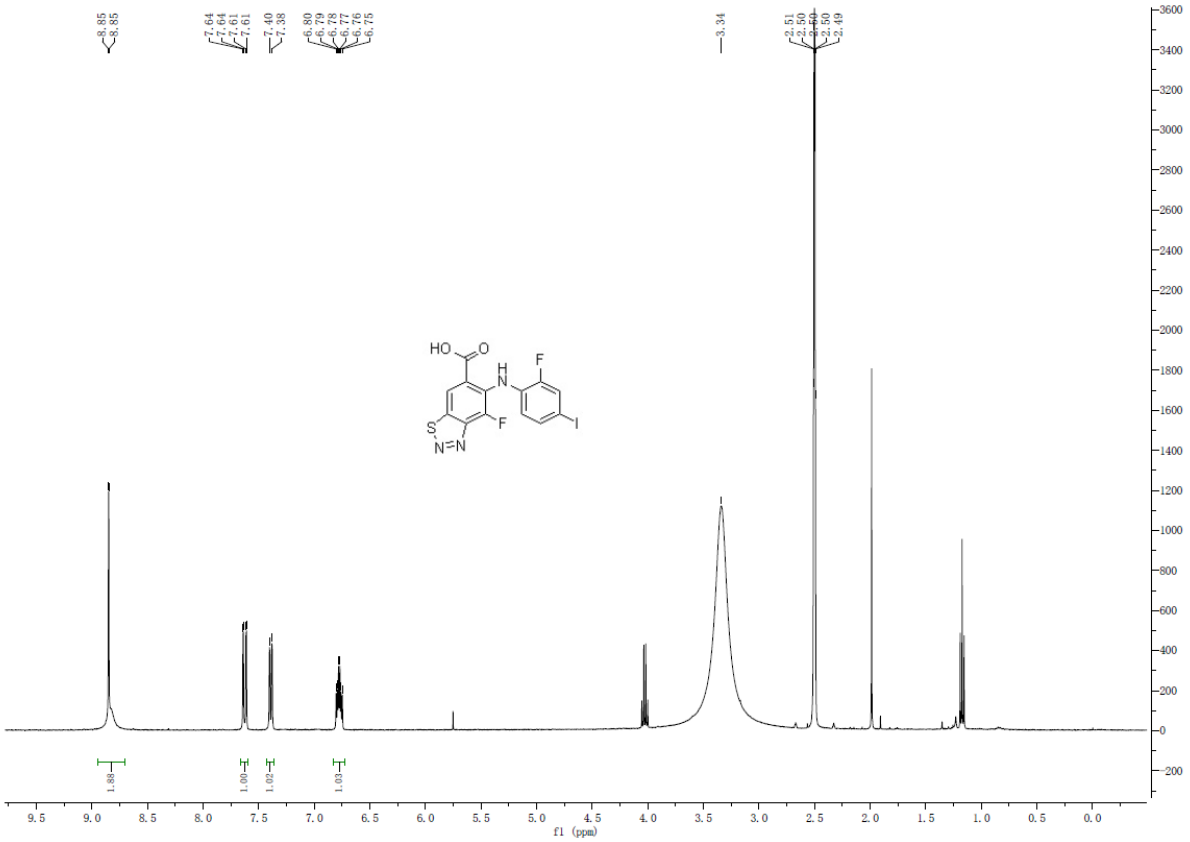

^{1}H NMR spectra of **KZ-02**

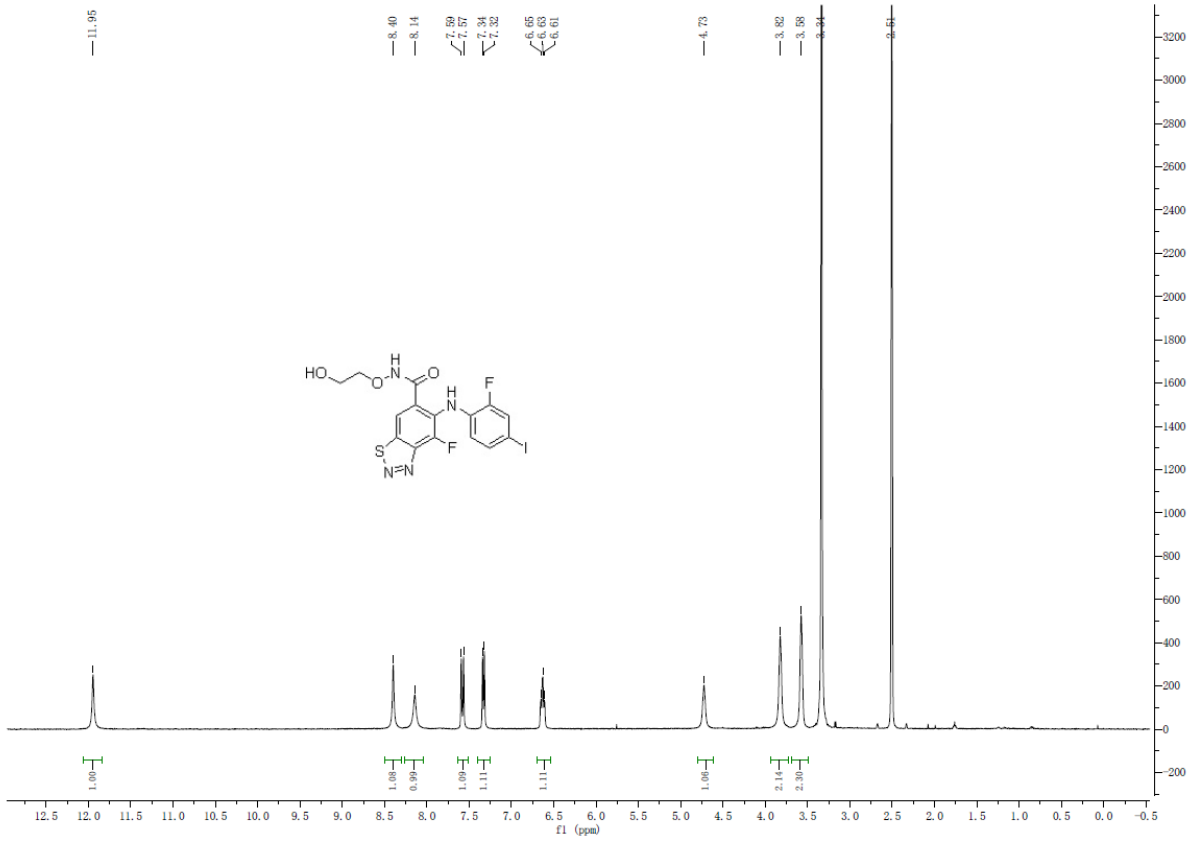

^{13}C NMR spectra of **KZ-02**

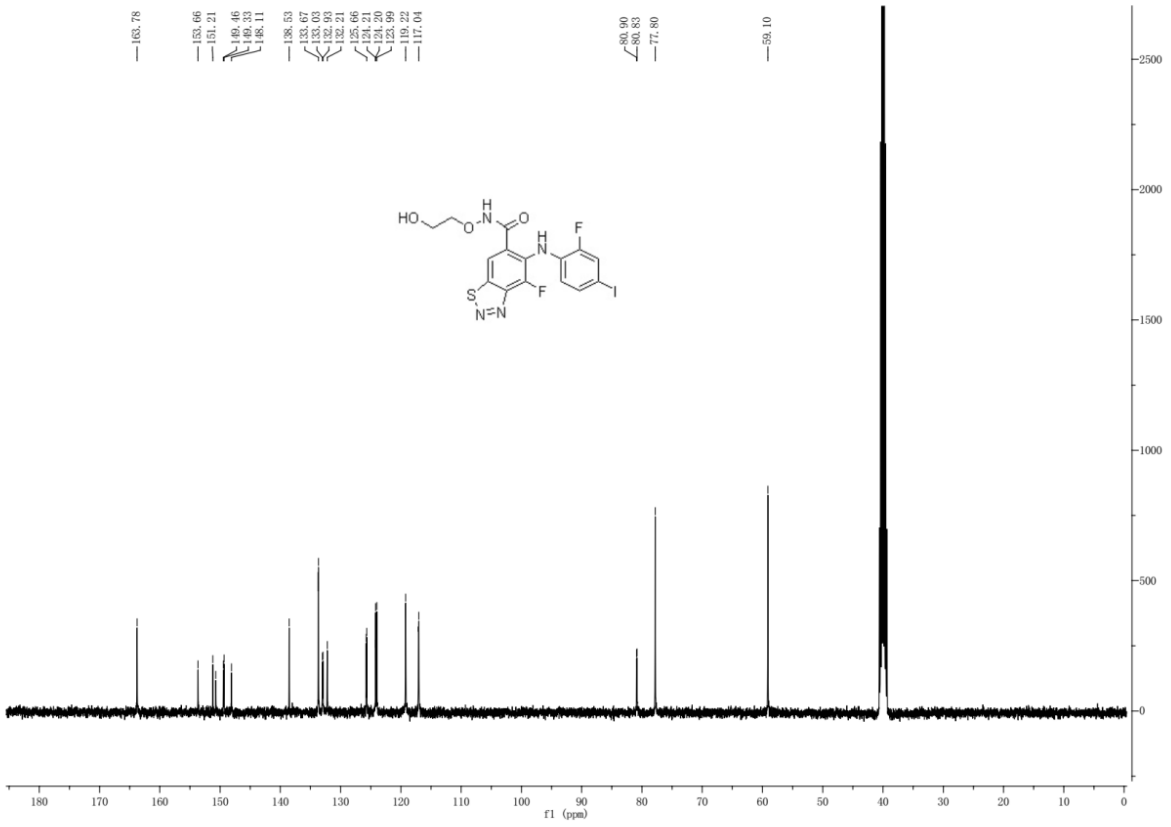

MS spectra of **KZ-02**

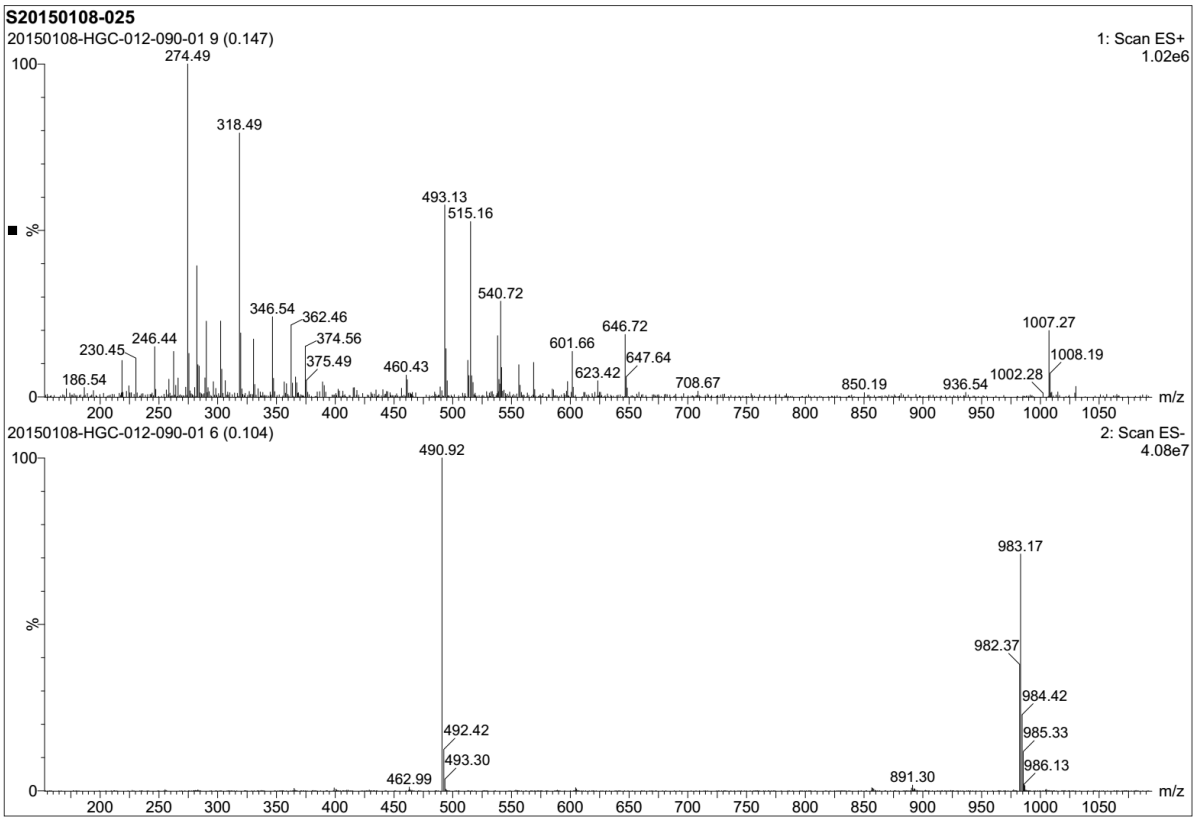

HRMS Spectra of **KZ-02**

Elmt	Val.	Min	Max	Elmt	Val.	Min	Max	Elmt	Val.	Min	Max	Elmt	Val.	Min	Max	Use Adduct
H	1	0	11	18O	2	0	0	P	3	0	0	Se	2	0	0	H
B	3	0	0	F	1	2	2	S	2	1	1	Br	1	0	0	Na
C	4	0	15	Na	1	0	0	Cl	1	0	0	I	3	1	1	K
N	3	0	4	Mg	2	0	0	Ti	2	0	0					NH4
O	2	0	3	Si	4	0	0	Fe	2	0	0					Br

Error Margin (ppm): 500
HC Ratio: 0.0 - 3.0
Max Isotopes: all
MSn Iso RI (%): 75.00

DBE Range: 0.0 - 50.0
Apply N Rule: yes
Isotope RI (%): 1.00
MSn Logic Mode: AND

Electron Ions: both
Use MSn Info: yes
Isotope Res: 10000
Max Results: 50

Event#: 1 MS(E+) Ret. Time : 0.613 -> 0.640 Scan# : 93 -> 97

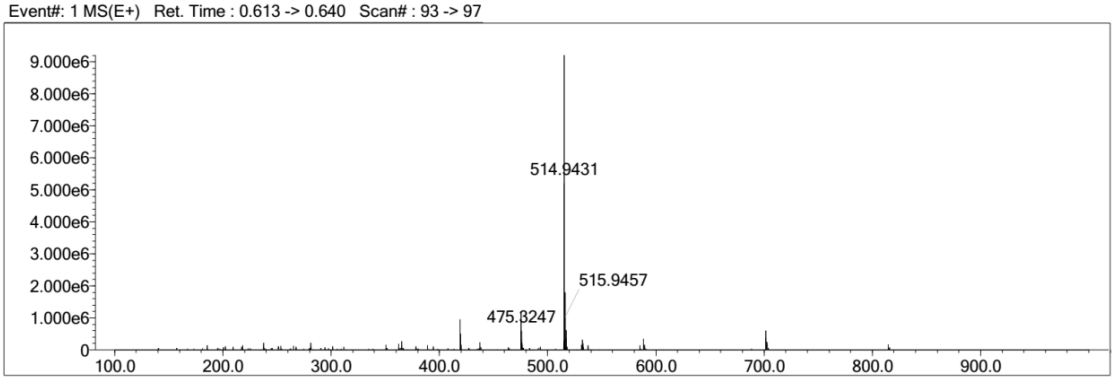

Measured region for 514.9431 m/z

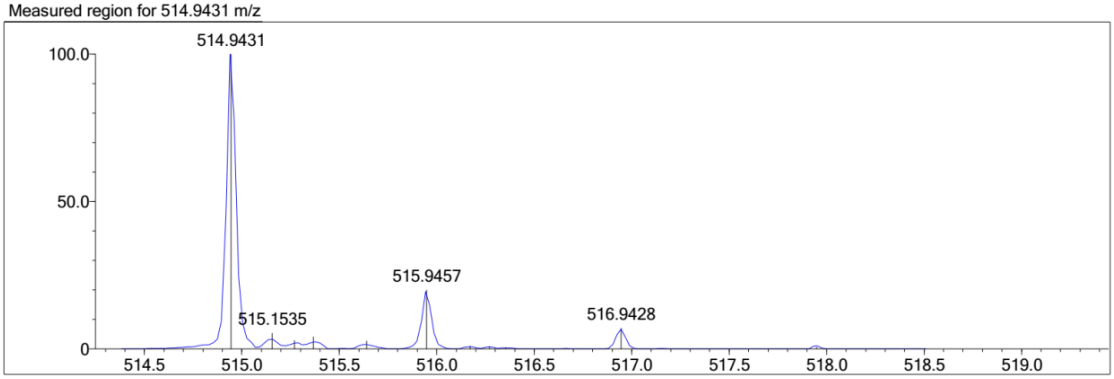

C15 H11 N4 O3 F2 S I [M+Na]+ : Predicted region for 514.9457 m/z

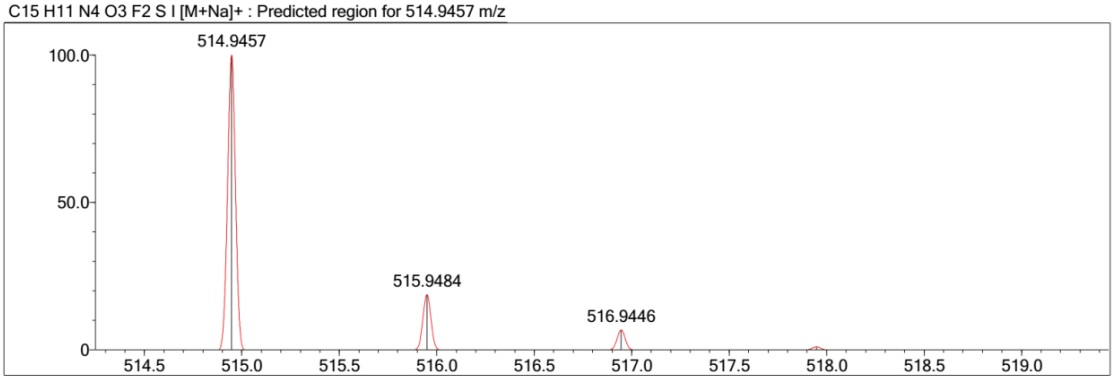

Rank	Score	Formula (M)	Ion	Meas. m/z	Pred. m/z	Df. (mDa)	Df. (ppm)	Iso	DBE
1	76.57	C15 H11 N4 O3 F2 S I	[M+Na]+	514.9431	514.9457	-2.6	-5.05	85.55	12.0

HPLC Spectra of **KZ-02**

Instrument & Column: HPLC-01(11#-603) Xbriage RP18, 5um

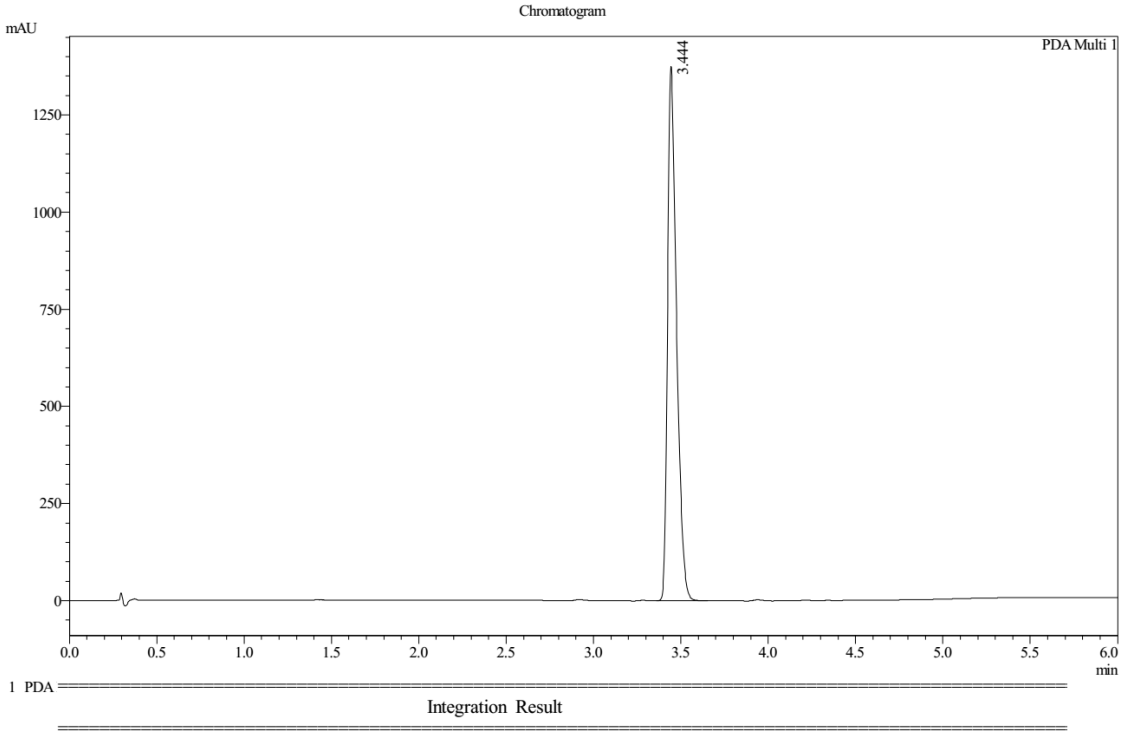

PDA Ch1 220nm 4nm

Peak#	Ret. Time	Height	Height %	USP Width	Area	Area %
1	3.444	1335027	100.000	0.097	4925937	100.000

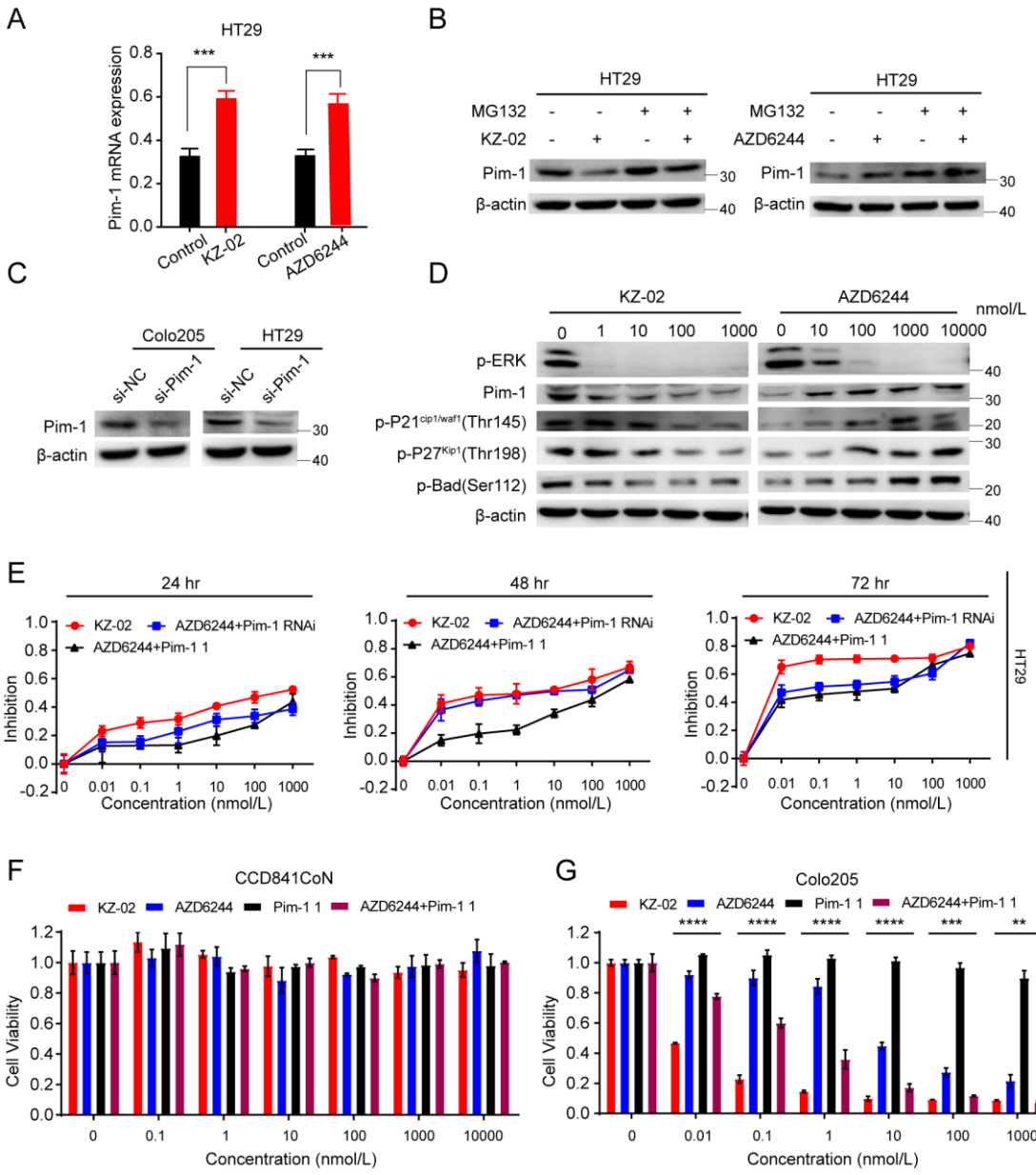

Figure S2. KZ-02 Inhibits Pim-1 Activation in HT29 Cells and Specifically Targets Tumor Cells. Related to Figure 7.

(a, b, d, e) Same experiments in HT29 cells as showed in Figures 7b-7e, which were in Colo205 cells. Error bars are based on the standard deviations of triplicate samples.
(c) Pim-1 protein levels after being knocked down were detected by western blot analysis.
(f, g) Benign colon cell CCD841CoN (f) or malignant colon cell Colo205 (g) were treated with various concentrations of KZ-02, AZD6244, Pim-1 1 or AZD6244+Pim-1 1 for 48 h, and cell proliferation inhibition was then determined by MTT assay. Error bars are based on the standard deviations of triplicate samples. Data are represented as mean ± SD. Comparisons of two groups are performed with Student's t-test. *P<0.05, **P<0.01, ***P<0.001,****P<0.0001.

SUPPLEMENTAL TABLE

Table S1. *In Vitro* Kinase Selectivity Screening for KZ-02. Related to Figure 3.

Kinase	% inhibition	Kinase	% inhibition	Kinase	% inhibition	Kinase	% inhibition
MEK1/MAP2K1	**100**	ERK2 (P42MAPK)	21	Ron kinase	6	IGF1R kinase	6
ALK	-1	ERK5 (MAPK7)	14	Src kinase	-8	IRK (InsR)	3
AKT1/PKBalpha	2	FAK	34	TIE2 kinase	3	IRR kinase	15
AKT2/PKBbeta	4	FGFR1 kinase	10	mTOR kinase (FRAP1)	1	JAK1	18
AKT3/PKBgamma	7	FGFR2 kinase	22	TRKA	-2	JAK2	4
ALK4 (ACVR1B)	33	MusK	26	TRKB	11	JAK3	9
AurA/Aur2 kinase	26	p38alpha kinase	7	TRKC	23	JNK1	16
AurC/Aur3 kinase	0	p38beta 2 kinase	-7	Tyk2 (JTK1)	11	JNK2	38
Axl kinase	1	p70S6K	15	MKK6 /p38alpha	26	JNK3	18
CHK1	-2	p70S6Kbeta	13	FGFR3 kinase	17	KDR kinase (VEGFR2)	3
CHK2	8	PDGFRalpha kinase	6	Tyro3 /Sky kinase	25	Lck kinase	-14
c-kit kinase	15	PDGFRbeta kinase	-1	FGFR4 kinase	4	LTK	-10
c-Met kinase	14	**Pim-1 kinase**	**89**	FLT-1 kinase (VEGFR1)	20	Lyn A kinase	3
DDR2 kinase	6	Pim-2 kinase	35	FLT-3 kinase	-4	Lyn B kinase	-2
EGFR kinase	20	PKA	-2	FLT-4 kinase (VEGFR3)	27	MEK5 (MAP2K5)	16
EphA1 kinase	7	PKCalpha	-15	Fms/CSFR kinase	14	Abl kinase	-7
EphA2 kinase	-15	RAF-1 kinase	33	GSK3alpha	64	Mer kinase	-2
EphB1 kinase	10	Ret kinase	10	GSK3beta	16		
EphB2 kinase	5	ROCK1	1	HER2/ErbB2 kinase	-29		
ERK1	1	ROCK2	2	HER4/ErbB4 kinase	3		

TRANSPARENT METHODS

Inhibitors, antibodies and reagents. KZ-02 was synthesized according to the scheme in the **Figure S1.** AZD6244 (MEK inhibitor, catalog No.S1008, purity >98%) was purchased from Selleck Chemicals. Pim-1 1 (Pim-1 inhibitor, sc-204330, purity >98%) was purchased from Santa Cruz Biotechnology. Compound C (AMPK inhibitor, S7840, purity >98%) was purchased from Selleck Chemicals. Recombinant human IL-23 (catalog#200-23, Lot#07125227, 10 μg) was purchased from PeproTech.

Immunoblotting was performed using the following antibodies: β-actin (sc-47778, Santa Cruz, dilution 1:5000), phospho-ERK1/2 (Thr202/Tyr204) (#4370, Cell Signaling, dilution 1:2000), ERK1/2 (#4695, Cell Signaling, dilution 1:1000), phospho-AMPK (Thr172) (#2535S, Cell Signaling, dilution 1:1000), AMPK (#5831S, Cell Signaling, dilution 1:1000), phospho-STAT3 (Tyr705) (#4113S, Cell Signaling, dilution 1:1000), STAT3 (#1264S, Cell Signaling, dilution 1:1000), Pim-1 (sc-28777, Santa Cruz, dilution 1:200), phospho-Cdc25C (Ser216) (#4901, Cell Signaling, dilution 1:1000), Cdc25C (#4688, Cell Signaling, dilution 1:1000), and GAPDH (#AM1020B, ABGENT, dilution 1:2000).

Lipofectamine®3000 transfection reagent (#L-3000-015) was purchased from Thermo Fisher Scientific. McCoy's 5A cell culture medium, 3-(4, 5-dimethyl-2-thiazolyl)-2, 5-diphenyl-2-H-tetrazolium bromide (MTT), SABC immunohistochemical kit, DAB color-developing reagent, methanol, isopropyl alcohol, dimethyl sulfoxide (DMSO) and other reagents were purchased from Sigma.

Cell lines and culture. All cells were originally purchased from the American Type Culture Collection (ATCC). Colo205 human colon cancer cells were cultured in Roswell Park Memorial Institute 1640 (RPMI-1640, Invitrogen) medium supplemented with 10% inactivated FBS. HT29 human colon cancer cells were grown in McCoy's 5A medium (Sigma) with the same supplementation. CCD841CoN human normal colon epithelial cells were maintained according to the recommendations of ATCC. All cells were routinely screened to avoid mycoplasma contamination and maintained in a humidified chamber with 5% CO_2 at 37^{o}C for up to 1 week after thawing before cell activity analysis or injection in mice.

Animals and tumor models. All mouse procedures were performed in accordance with institutional protocol guidelines at Shantou University. Male nude mice around 4 weeks obtained from Beijing Vital River Laboratory Animal Technology Co., Ltd. (China) were fed at laboratory animal center of Shantou University Medical College. Mice were treated with Colo205 or HT29 cells to

construct the tumor models. When the volume of each tumor was around 200 mm^3, sequential animal studies were carried out.

Clinical samples. Twenty paraffin-embedded specimens of CRC preserved at the Department of Pathology of Shantou University Medical College Cancer Hospital between January 2010 and August 2015 were included in this study. Specimens were examined for histological grade based on World Health Organization criteria. All specimens were fixed with paraformaldehyde, embedded in paraffin, and prepared as serial slices of 4 μm in thickness. All experimental subjects had complete clinical pathological data and were aged 45-75 years (mean: 58.65), and there were no significant differences between age groups. No patients received radiotherapy, chemotherapy, biotherapy, or any other operation before surgery for the cancer. The pathological diagnosis was performed by experts at the Department of Pathology of Shantou University Medical College Cancer Hospital. All procedures involved in this clinical trial were in compliance with the ethical regulations. Any study-related clinical procedures and the acquisition of clinical samples or data were performed after the patient signed an approved informed consent. Patient samples were collected according to the study protocol approved by the institutional review boards of Shantou University Medical College Cancer Hospital.

Preparation of KZ-02. The target compound was synthesized under 11 steps. The initial compounds of 1-bromo-2,3,4-trifluorobenzene and 2-fluoroaniline were purchased from Shanghai Bidepharmatech Chemical.

<Step 1: 5-bromo-2,3,4-trifluorobenzoic acid (Compound1)>Under N_2 atmosphere, 1-bromo-2,3,4-trifluorobenzene (13.64 g, 64.6 mmol) was dissolved in 120 mL anhydrous THF. The solution was cooled to –78 ^oC, and then LDA (2.0 M in THF, 33.9 mL, 67.97 mmol) was added dropwise. The mixture was stirred at this temperature for an additional 1 h, and then poured into dry ice carefully. The mixture was warmed to r.t and stirred for 1 h. The pH of the solution was adjusted to 2 – 3 with 10% HCl (300 mL), and extracted with ethyl acetate (200 mL×3). The organic phase was washed with brine, dried over anhydrous Na_2SO_4, filtered and concentrated. The residue was washed with PE, filtrated, and dried to obtain compound **1** as a white solid (13.50 g, 82%). ^1H NMR (400 MHz, DMSO-d_6) δ 13.94 (s, 1H), 7.98 (t, J = 75.2 Hz, 1H).

<Step 2: 5-bromo-3,4-difluoro-2-((2-fluorophenyl)amino)benzoic acid (Compound 2)>Under N_2 atmosphere, to the solution of compound **1** (13.50 g, 52.9 mmoL) and 2-fluoroaniline (10.2 mL, 105.8 mmol) in 120 mL anhydrous THF at –78 ^oC, LiHMDS (1M in THF, 158.7 mL, 158.7 mmol) was added dropwise. The mixture was slowly warmed to r.t and stirred for 8 h. The mixture was quenched with 10% HCl

(aq., 100 mL) at 0 °C, extracted with ethyl acetate (200 mL×3). The organic layer was washed with brine, dried over anhydrous Na_2SO_4, filtered and concentrated. The residue was washed with PE, filtrated, and dried yielding to the desired compound **2** as a pale-yellow solid (13.73 g, 75%). ^{1}H NMR (400 MHz, DMSO-d_6) δ 9.22 (s, 1H), 8.00 (dd, *J* = 7.4, 2.1 Hz, 1H), 7.29 – 7.20 (m, 1H), 7.18 – 7.01 (m, 3H).

<Step 3: Methyl 5-bromo-3,4-difluoro-2-((2-fluorophenyl)amino)benzoate (Compound 3)>A solution of compound **2** (13.73 g, 39.6 mmol) in 60 mL thionyl chloride and 300 mL MeOH was stirred at 85 °C for 12 h. The solution was cooled to room temperature and concentrated to remove most MeOH. The residue was filtrated, washed with MeOH, dried yielding to the desired compound **3** as an off-white solid (12.58g, 90%). ^{1}H NMR (400 MHz, $CDCl_3$) δ 9.07 (s, 1H), 8.02 (dd, *J* = 7.1, 2.3 Hz, 1H), 7.17 – 6.95 (m, 4H), 3.93 (s, 3H).

<Step 4: Methyl 5-(benzylthio)-3,4-difluoro-2-((2-fluorophenyl)amino)benzoate (Compound 4)>Under N_2 atmosphere, to the solution of compound **3** (12.58 g, 35.80 mmol) in 30 mL 1,4-dioxane, phenylmethanethiol (4.44 g, 35.80 mmoL), DIPEA (9.21 g, 71.60 mmol), Xantphos (2.06 g, 3.56 mmol) and Tris (dibenzylideneacetone)dipalladium (1.63 g, 1.78 mmol) were added. After being stirred at 90°C for 8 h, the mixture was cooled to r.t, filtrated and washed with ethyl acetate. The organic phase was washed with brine, dried over anhydrous Na_2SO_4, filtered and concentrated. The residue was purified by silica gel column chromatography (PE/EA 50/1, v/v) to obtain the compound **4** as an off-white solid (12.64 g, 88%). ^{1}H NMR (400 MHz, $CDCl_3$) δ 9.11 (s, 1H), 7.75 (dd, *J* = 7.5, 2.1 Hz, 1H), 7.31 – 7.19 (m, 5H), 7.14 – 6.93 (m, 4H), 4.04 (s, 2H), 3.87 (s, 3H).

<Step 5: Methyl 4-azido-5-(benzylthio)-3-fluoro-2-((2-fluorophenyl) amino) benzoate (Compound 5)>To a solution of compound **4** (12.64 g, 31.36 mmol) in 30 mL DMA, NaN_3 (2.45 g, 37.63 mmol) was added. The mixture was heated to 90 °C and stirred for 3 h. After it was cooled to r.t, the mixture was poured into ice-water, extracted with ethyl acetate (100 mL×3). The organic phase was washed with brine, dried over anhydrous Na_2SO_4, filtered and concentrated. The residue was used for next step without purification (10.38 g, 78%). ^{1}H NMR (400 MHz, $CDCl_3$) δ 8.96 (s, 1H), 7.73 (s, 1H), 7.27 - 7.23 (m, 3H), 7.12 – 6.89 (m, 6H), 4.05 (s, 2H), 3.87 (s, 3H).

<Step 6: Methyl 4-amino-5-(benzylthio)-3-fluoro-2-((2-fluorophenyl)amino) benzoate (Compound 6)>Under N_2 atmosphere, to the solution of compound **5** (10.38 g, 24.36 mmol) in 100mL MeOH was added 10% Pd/C (1.55 g). The N_2 atmosphere was completely changed to H_2 atmosphere. The mixture was stirred at r.t for 6 hours. The mixture was filtrated and washed with MeOH. The organic phase was concentrated to give the compound **6** as an off-white solid, which was used for next without purification (9.79 g, 100%).

<Step 7: Methyl 4-fluoro-5-((2-fluorophenyl)amino)benzo[d][1,2,3]thiadiazole -6-carboxylate (Compound 7)>To a solution of compound **6** (2.07 g, 5.17 mmol) in acetic acid (60 mL), concentrated HCl (8 mL) and water (6 mL) were added. The mixture was stirred at r.t for 1 h, and then cooled to 5 – 10^{o}C with ice-water batch. The 10 mL solution of $NaNO_2$ (0.43 g, 6.21 mmol) in water was added dropwise to the mixture with the temperature less than 10 ^{o}C. At the end of the drip, the mixture was stirred at this temperature for an additional 3 h, and then adjusted the pH to 8 with sat. $NaHCO_3$, extracted with ethyl acetate (30 mL×3). The organic layer was washed with brine, dried over anhydrous Na_2SO_4, filtered and concentrated. The residue was purified by silica gel column chromatography (PE/EA 5/1) yielding to the compound **7** as a yellow solid (1.53 g, 92.1%). ^{1}H NMR (400 MHz, $CDCl_3$) δ 8.73 (s, 1H), 8.55 (d, *J* = 1.5 Hz, 1H), 7.17 – 7.10 (m, 1H), 7.10 – 7.04 (m, 1H), 7.04 – 6.95 (m, 2H), 4.01 (s, 3H). MS (ESI): m/z: 322.31 $[M+H]^+$.

<Step 8: Methyl 4-fluoro-5-((2-fluoro-4-iodophenyl)amino)benzo[d][1,2,3] thiadiazole-6-carboxylate (Compound 8)>To a solution of compound **7** (1.53 g, 4.77 mmol) in 10 mL DMF, NIS (1.18 g, 5.24 mmol) and trifluoroacetic acid (0.5 mL) was added. The mixture was stirred at r.t for 4 h, and then quenched with sat. aq NH_4Cl, extracted with ethyl acetate (30 mL×3). The organic phase was washed with brine (30 mL×3), dried over anhydrous Na_2SO_4, filtered and concentrated to obtain the compound **8** as a yellow solid (1.90 g, 89%). ^{1}H NMR (400 MHz, $CDCl_3$) δ 8.71 (s, 1H), 8.56 (d, *J* = 1.5 Hz, 1H), 7.46 (dd, *J* = 10.3, 1.9 Hz, 1H), 7.37 (d, *J* = 8.5 Hz, 1H), 6.71 (td, *J* = 8.6, 5.9 Hz, 1H), 4.01 (s, 3H).

<Step 9: 4-fluoro-5-((2-fluoro-4-iodophenyl)amino)benzo[d][1,2,3]thiadiazole-6 -carboxylic acid (Compound 9)>The compound 8 (1.90 g, 4.25 mmol) was dissolved in the THF/MeOH = 4/1(v/v) (20 mL), and then10 mL of 1M LiOH (10.00 mmol) was added to the solution. The mixture was stirred at r.t for 2 h. Adjusted the pH to 3–4 with 10% HCl, and extracted with ethyl acetate. The organic phase was washed with brine, dried over anhydrous Na2SO4, filtered and concentrated to obtain the compound **9** as a brown yellow solid (1.70 g, 94.0%). ^{1}H NMR (400 MHz, DMSO-d_6) δ 8.85 (d, *J* = 0.9 Hz, 2H), 7.63 (dd, *J* = 10.9, 1.9 Hz, 1H), 7.39 (d, *J* = 8.5 Hz, 1H), 6.78 (td, *J* = 8.9, 5.0 Hz, 1H).

<Step 10: 4-fluoro-5-((2-fluoro-4-iodophenyl)amino)-N-(2-(vinyloxy)ethoxy)benzo [d][1,2,3]thiadiazole-6-carboxamide (Compound 10)>To a solution of compound **9** (1.7 g, 5.54 mmoL) in 20 mL DCM, EDCI (1.59 g, 8.31 mmol) and HOBT (1.21 g, 8.31 mmol) were added. The solution was stirred at r.t for 10 min and then O-(2-(vinyloxy) ethyl) hydroxylamine (0.69 g, 6.65 mmol) was added. The mixture was stirred at r.t for 4 h, and then quenched with sat. aq NH_4Cl (20 mL), extracted with DCM (15 mL×3). The organic phase was washed with brine, dried over

anhydrous Na_2SO_4, filtered and concentrated to obtain the compound **10** (2.44g, 85%), which was used for the next step without further purification.

<Step 11: 4-fluoro-5-((2-fluoro-4-iodophenyl)amino)-N-(2-hydroxyethoxy) benzo[d] [1,2,3] thiadiazole-6-carboxamide (KZ-02)> To a solution of compound **10** (410 mg, 0.79 mmoL) in 5 mL DCM, 5.0 mL of 1 M HCl (5.0 mmol) was added. The mixture was stirred at r.t for 1 h. The mixture was diluted with sat. aq $NaHCO_3$, extracted with DCM. The organic phase was washed with brine, dried over anhydrous Na_2SO_4, filtered and concentrated. The residue was purified by silica gel column chromatography (DCM/MeOH 20/1) yielding to the final compound **KZ-02** as a yellow solid (343 mg, 88%). ^{1}H NMR (400 MHz, DMSO-d_6) δ 11.95 (s, 1H), 8.40 (s, 1H), 8.14 (s, 1H), 7.58 (d, *J* = 11.1 Hz, 1H), 7.33 (d, *J* = 8.4 Hz, 1H), 6.63 (t, *J* = 7.5 Hz, 1H), 4.73 (s, 1H), 3.82 (s, 2H), 3.58 (s, 2H). ^{13}C NMR (101 MHz, DMSO-d_6) δ 163.78, 153.66 - 151.21 , 150.71-148.11, 149.39 , 148.11 , 138.53 , 133.67, 132.21, 125.71 , 124.10 , 119.22, 117.04, 80.86, 77.80 , 59.10 .. MS (ESI): m/z: 493.13 $[M+H]^+$; HRMS, $[M+Na]^+$ for $C_{15}H_{11}F_2IN_4O_3S$, calcd, 514.9457; found, 514.9431. HPLC: 100%.

The synthetic route was shown schematically in **Figure S1.** The target compound and key intermediates had been precisely characterized by reasonable testing methods including ^{1}H NMR (nuclear magnetic resonance), ^{13}C NMR, MS (mass spectrum), HRMS (high resolution mass spectrum), or HPLC (high performance liquid chromatography). The results were shown in Data S1.

***In vitro* cell proliferation assay.** MTT assays were performed using a Cell Proliferation Kit (Sigma) following the supplier's instructions. Briefly, Colo205 cells (2×10^3) were inoculated into each well of a 96-well plate. After being cultured for 24 h, the cells were treated with 0.01 nmol/L to 1000 nmol/L of KZ-02, AZD6244, Pim-1 1, AZD6244+Pim-1 1 (1:1) or DMSO control for 24, 48 and 72 h. Medium was then changed and replaced with 100 μL of fresh growth medium with 10% FBS and 20 μL of 5 mg/mL MTT solution. Cells were incubated for another 4 h, and the medium was replaced with 150 μL of DMSO. After 15 min of incubation at 37ºC, the optical absorbance at 570 nm was measured using a micro-plate reader. Results were presented as the percentage of cell inhibition. Data collected at 0 nmol/L was set to 0 in each panel.

The coefficient of drug interaction (CDI) was used to analyze the synergistic inhibitory effect of drug combinations and calculated according to the reported literature (Wang et al., 2008). CDI was calculated as follows: CDI = AB/(A ×B). According to the absorbance of each group, AB was the ratio of the combination group to the control group, A or B was the ratio of the single agent groups to the control group. Thus, a CDI value less than, equal to or greater than 1 indicates that the

drugs are synergistic, additive or antagonistic, respectively. A CDI of less than 0.7 indicates that the drugs are significantly synergistic.

***In vivo* mouse tumor injection and growth assay.** All animal experiments strictly adhered to local and federal regulations, and were approved by the local authorities before initiation. Balb/c mice weighing 20 g were inoculated subcutaneously with 1×10^7 Colo205 or HT29 cells in 100 μL of a serum-free media and Matrigel mixture (BD Biosciences, 1:1). When the tumors reached about 200 mm^3, tumor-bearing mice were separated into treatment groups of eight mice each, and the indicated inhibitor treatments were performed by oral gavage once daily (QD) for 20 days. The treatment groups consisted of vehicle (20% sulfobutyl ether-β-cyclodextrin (SBE-β-CD) in water), KZ-02 (1 mg/kg for Colo205), AZD6244 (10 mg/kg for Colo205, 20 mg/kg for HT29), Pim-1 1 (20 mg/kg for HT29), and AZD6244+Pim-1 1 (20 mg/kg for HT29). Tumor sizes were recorded every 3 days for 21 days by caliper, and volumes were calculated using the formula of (length × $width^2$)/2. Body weights were also determined at the same time points.

Kinase selectivity screening and kinase 50% inhibitory concentration (IC_{50}) determination *in vitro*. Screening for inhibitory activity against various kinases and the examination of IC_{50} of KZ-02 and AZD6244 against MEK1 and Pim-1 were completed by Cerep Drug Discovery Services Co. LTD (France).

Western blot analysis. Immunoblot analysis was performed as previously reported (Landriscina et al., 2010) and improved appropriately. Cells were washed with ice-cold PBS (phosphate-buffered saline), and resuspended in lysis buffer (20 mmol/L Tris(hydroxymethyl)aminomethane-HCl, pH=7.5, containing 1% sodium dodecyl sulfate (SDS), 50 mmol/L NaCl, 1 mmol/L ethylenediaminetetraacetic acid, 1 mmol/L phenylmethylsulfonyl fluoride, 10 mmol/L sodium fluoride, and 1 mmol/L sodium orthovanadate) by agitation at 4 ℃ for 1 h followed by centrifugation at 4 ℃, 11000 g for 15 min. Equal amounts (20 μg protein) of supernatant were then subjected to SDS-polyacrylamide gel electrophoresis (PAGE) and the separated proteins transferred to nitrocellulose membranes. Membranes were routinely blocked in 5% nonfat milk in Tris-buffered saline (TBS) with 0.1% Tween-20 (TBST) for 1 h at room temperature with agitation and washed. Primary antibodies, including phospho-ERK1/2 (Thr202/Tyr204), ERK1/2, phospho-AMPK (Tyr172), AMPK, phospho-STAT3 (Tyr705), STAT3, Pim-1, phospho-Cdc25C (Ser216), Cdc25C, β-actin, and GAPDH, were added (diluted in 5% bovine serum albumin (BSA) in TBST). Membranes were incubated overnight at 4 ℃ with agitation, washed, and then incubated with horseradish peroxidase-conjugated secondary antibodies (1:5000 dilution in 5% BSA in TBST) for 1 h at room temperature. Proteins were detected

using Enhanced Chemiluminescence Western Blotting Detection Reagent (GE Healthcare). Results were visualized and quantified by an ImageQuant LAS 4000 (GE Healthcare). Protein analysis of tumor tissue lysate was conducted following the same protocol, using protein extraction from tumors pretreated by AZD6244, Pim-1 1, or their combination for 15 days with blank vehicles as control.

Immunohistochemistry (IHC). Formalin-fixed paraffin-embedded tissue slices were treated according to manual of the SABC immunohistochemical kit, and results were analyzed using a double-blind method. Five high-power fields (×400) were selected at random, and two pathologists evaluated scores independently. PBS, instead of the primary antibody, was used as negative control, and specimens were scored according to the intensity of the dye color and the number of positive cells. The intensity of the dye color was graded as 0 (no color), 1 (light yellow), 2 (light brown), or 3 (brown), and the number of positive cells was graded as 0 (<1%), 1 (1-24%), 2 (25-49%), 3 (50-74%), or 4 (75-100%). The two grades were added together and specimens were assigned to one of 4 levels: 0-2 scores (-), 3-5 scores (+), 6-8 scores (++), 9-12 scores (+++). The positive expression rate was expressed as the percent of the addition of (++) and (+++) to the total number.

Quantitative real-time PCR (RT-PCR). RT-PCR was performed as described previously (Maddalena et al., 2011). Total RNA was extracted from cultured cells with TRIzol, and reverse transcription of purified RNA was performed using oligo (dT) priming and Superscript III reverse transcription according to the manufacturer's instructions (Invitrogen). Quantification of all gene transcripts was performed by quantitative PCR using the SYBR Premix kit (TaKaRa) and a Rotor-Gene RG-3000A apparatus (Corbett Research). The gene expressions were all normalized by GAPDH. Data were analyzed by applying the $2^{-\Delta C_T}$ calculation method. The primer pairs used for target gene amplification were as follows: human Pim-1: forward 5'-CCGAGTGTATAGCCCTCCAG-3', and reverse 5'-GGGCCAAGCACCATCTAATG-3', human IL-8: forward 5'-TTCAGAGACAGCAGAGCACA-3', and reverse 5'-AGCACTCCTTGGCAAAACTG-3', human IL-10: forward 5'-AAGGCGCATGTGAACTCCC-3', and reverse 5'-ACGGCCTTGCTCTTGTTTTC-3', human IL-16: forward 5'-TAGAATCTACAGCAGAGGCCA-3', and reverse 5'-TTTGTTCTGAGGCTGCTCCTT-3', human IL-23: forward 5'-CTCTGCTCCCTGATAGCCCT-3', and reverse 5'-TGCGAAGGATTTTGAAGCGG-3', GAPDH: forward 5'-AGGTCGGAGTCAACGGATTT-3', and reverse

5’-ATCTCGCTCCTGGAAGATGG-3’.

Transfection. siRNAs specific for ERK1, ERK2, Pim-1, and IL-23 used in this study were previously described (Ma et al., 2017; Steinmetz et al., 2004; Zhang et al., 2010) and synthesized by Shanghai GenePharma Co. Ltd. with the following target sequences: 5’-GACCGGAUGUUAACCUUUA-3’, 5’-GGUGUGCUCUGCUUAUGAU-3’, 5’-AGAACAUCUUGCAUCCAUGGAUGGU-3’, and 5’-AAUCUGCUGAGUCUCCCAGUGGUGA-3’ respectively. SiRNAs were transfected at 100 pmol per well (6-well plate). Cells were inoculated in plates and allowed to attach for 18-24 h, followed by transfection with siRNAs by Lipofectamine RNAiMAX according to the manufacturer’s protocols. At 48 h after transfection, cells were lysed for protein expression analysis by western blot.

Statistical analyses. Statistical analyses were performed on the GraphPad Prism 7 software, using two-sided Student’s t-test and two-way analysis of variance to detect statistically significant differences between groups. Detailed statistical procedure and data distribution used in each experiment was reported in respective figure legend. P values were calculated to visually indicate the statistical results, and the significance was defined as follows: *P<0.05, **P<0.01, ***P<0.001,****P<0.0001.

SUPPLEMENTAL REFERENCES

Landriscina, M., Laudiero, G., Maddalena, F., Amoroso, M.R., Piscazzi, A., Cozzolino, F., Monti, M., Garbi, C., Fersini, A., Pucci, P., *et al.* (2010). Mitochondrial chaperone Trap1 and the calcium binding protein Sorcin interact and protect cells against apoptosis induced by antiblastic agents. Cancer Res. *70*, 6577-6586.

Maddalena, F., Laudiero, G., Piscazzi, A., Secondo, A., Scorziello, A., Lombardi, V., Matassa, D.S., Fersini, A., Neri, V., Esposito, F., *et al.* (2011). Sorcin induces a drug-resistant phenotype in human colorectal cancer by modulating Ca(2+) homeostasis. Cancer Res. *71*, 7659-7669.

Ma, N., Yang, D., Okamura, H., Teramachi, J., Hasegawa, T., Qiu, L., and Haneji, T. (2017). Involvement of interleukin23 induced by Porphyromonas endodontalis lipopolysaccharide in osteoclastogenesis. Mol. Med. Rep. *15*, 559-566.

Steinmetz, R., Wagoner, H.A., Zeng, P., Hammond, J.R., Hannon, T.S., Meyers, J.L., and Pescovitz, O.H. (2004). Mechanisms regulating the constitutive activation of the extracellular signal-regulated kinase (ERK) signaling pathway in ovarian cancer and the effect of ribonucleic acid interference for ERK1/2 on cancer cell proliferation. Mol. Endocrinol. *18*, 2570-2582.

Wang, D., Wang, Z., Tian, B., Li, X., Li, S., and Tian, Y. (2008). Two hour exposure to sodium butyrate sensitizes bladder cancer to anticancer drugs. Int. J. Urol. *15*, 435-441.

Zhang, T., Zhang, X., Ding, K., Yang, K., Zhang, Z., and Xu, Y. (2010). PIM-1 gene RNA interference induces growth inhibition and apoptosis of prostate cancer cells and suppresses tumor progression in vivo. J. Surg. Oncol. *101*, 513-519.